Cell Reports

Article

macroH2A1 drives nucleosome dephasing and genome instability in histone humanized yeast

Graphical abstract

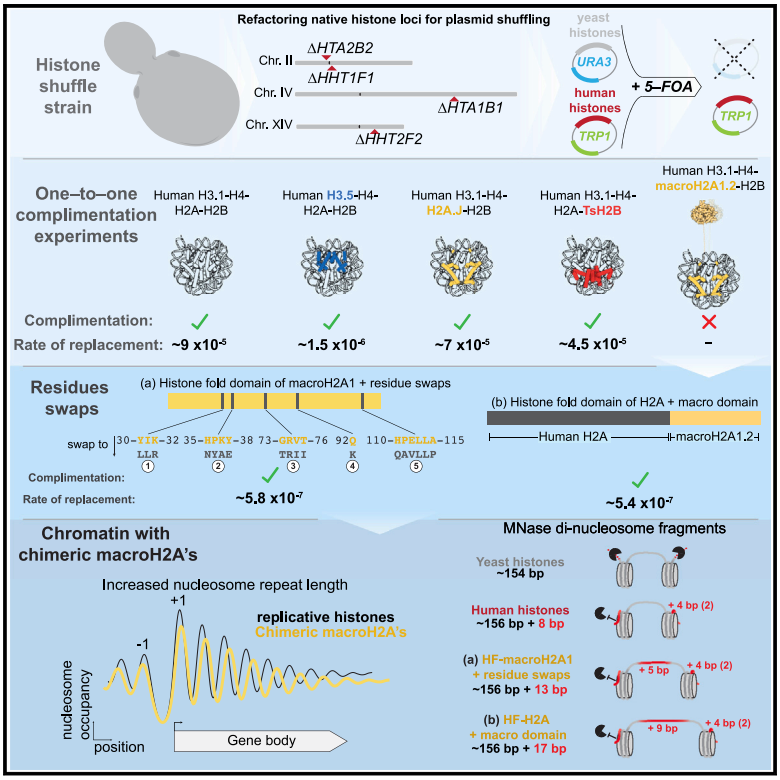

Highlights

- Expanded toolset for swapping histones in *S. cerevisiae*
- Complementation tests between human replicative histones and their variants
- Amino acid swapping experiments between replicative human H2A and macroH2A1.2
- Human macroH2A1.2 alters the structure of yeast chromatin fiber locally and at long range

Authors

Max A.B. Haase, Luciana Lazar-Stefanita, Guðjón Ólafsson, Aleksandra Wudzinska, Michael J. Shen, David M. Truong, Jef D. Boeke

Correspondence

jef.boeke@nyulangone.org

In brief

Haase et al. used a genetic swapping assay to replace replicative human histones with non-replicative variants in yeast. H2A.J, TsH2B, and H3.5 complemented their replicative counterparts, while macroH2A1.2 proved toxic, disrupting chromatin organization, increasing nucleosome repeat length, and—when associated with chromosome instability—leading to fitness defects in yeast.

Haase et al., 2024, Cell Reports *43*, 114472
July 23, 2024
https://doi.org/10.1016/j.celrep.2024.114472

CellPress

Cell Reports

CellPress
OPEN ACCESS

Article

macroH2A1 drives nucleosome dephasing and genome instability in histone humanized yeast

Max A.B. Haase,[1,2,5] Luciana Lazar-Stefanita,[1] Guðjón Ólafsson,[1,6] Aleksandra Wudzinska,[1] Michael J. Shen,[1,7] David M. Truong,[3,4] and Jef D. Boeke[1,3,8,*]

[1]Institute for Systems Genetics and Department of Biochemistry and Molecular Pharmacology, NYU Langone Health, New York, NY 10016, USA
[2]Vilcek Institute of Graduate Biomedical Sciences, NYU School of Medicine, New York, NY 10016, USA
[3]Department of Biomedical Engineering, NYU Tandon School of Engineering, Brooklyn, NY 11201, USA
[4]Department of Pathology, NYU Langone Health, New York, NY 10016, USA
[5]Present address: Department of Mechanistic Cell Biology, Max Planck Institute of Molecular Physiology, Dortmund, Germany
[6]Present address: Department of Biochemistry and Molecular Biology, Faculty of Medicine, BioMedical Center, University of Iceland, Reykjavik, Iceland
[7]Present address: Hospital of the University of Pennsylvania, Division of Gastroenterology and Hepatology, Philadelphia, PA, USA
[8]Lead contact
*Correspondence: jef.boeke@nyulangone.org
https://doi.org/10.1016/j.celrep.2024.114472

SUMMARY

In addition to replicative histones, eukaryotic genomes encode a repertoire of non-replicative variant histones, providing additional layers of structural and epigenetic regulation. Here, we systematically replace individual replicative human histones with non-replicative human variant histones using a histone replacement system in yeast. We show that variants H2A.J, TsH2B, and H3.5 complement their respective replicative counterparts. However, macroH2A1 fails to complement, and its overexpression is toxic in yeast, negatively interacting with yeast's native histones and kinetochore genes. To isolate yeast with macroH2A1 chromatin, we uncouple the effects of its macro and histone fold domains, revealing that both domains suffice to override native nucleosome positioning. Furthermore, both uncoupled constructs of macroH2A1 exhibit lower nucleosome occupancy, decreased short-range chromatin interactions (<20 kb), disrupted centromeric clustering, and increased chromosome instability. Our observations demonstrate that lack of a canonical histone H2A dramatically alters chromatin organization in yeast, leading to genome instability and substantial fitness defects.

INTRODUCTION

The basic repeating unit of eukaryotic chromatin is the nucleosome core particle[1]; approximately 146 bp of DNA wrap around a histone octamer comprising a tetramer of histone H3 and H4 and two dimers of histones H2A and H2B.[2] Replicative histones package the bulk of DNA, are regulated in a cell-cycle-specific manner, and are typically encoded in multicopy gene clusters.[3] The conserved role of replicative histones in DNA packaging and regulation is apparent by their high sequence identity in divergent species.[4,5] In contrast, non-replicative variant histones are distinct genes, separated from the replicative histone clusters, and as the name suggests, regulated independently of the cell cycle.[6] Typically, variant histones have selective chromatin deposition/eviction mechanisms linked to specific chromatin remodelers and chaperones.[7,8] Certain histone variants are considered "universal" as they diverged before the diversification of eukaryotes (CenH3, H3.3, H2A.Z, and H2A.X) and are broadly found in most species, such as CenH3, whose role is in maintaining centromeric chromatin for chromosome segregation.[9] In contrast, some ancient histone variants have been differentially lost throughout evolution, such as macroH2A's in fungi, which evolved long ago in premetazoan protists—before the divergence of metazoans and fungi—and was lost in the latter.[10] Histone variants have continually emerged throughout evolution via gene duplication as in the case of macroH2A2 in the basal roots of vertebrate evolution[11] or via duplication and rapid diversification of short H2As in eutherian mammals.[12] Budding yeasts have a surprisingly small complement of variant histones, especially in contrast to a species such as humans (Figure 1A). The budding yeast *Saccharomyces cerevisiae* minimally encodes a centromeric-specific H3 (Cse4), which defines its point centromeres, an H2A.Z variant (Htz1) that localizes to either side of the nucleosome-depleted region (NDR) near transcription start sites (TSSs), and a histone H1

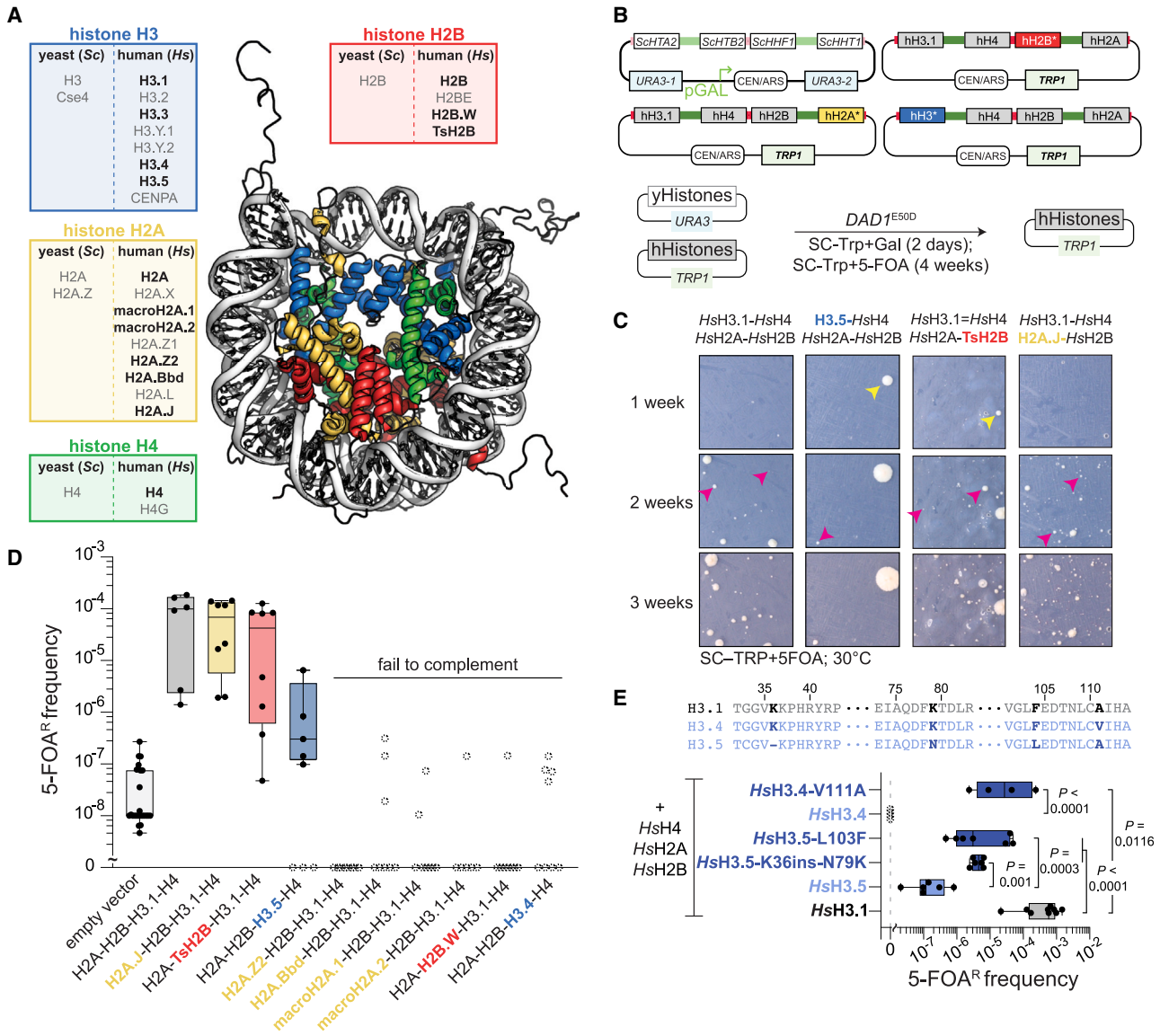

Figure 1. Complementation of human replicative histones with their variant histone counterparts in yeast

(A) Overview of human histone variants examined in this study (bolded) and other variants not studied. Nucleosome core particle is shown (PDB: 1KX5).

(B) Overview of histone humanization assay (STAR Methods for details).

(C) Exemplar images of histone humanization assay at three time points (growth at 30°C). Yellow arrows denote large colonies that emerged early (within 1 week of growth), and pink arrows denote small colonies that emerged at ~2 weeks of growth.

(D) Quantification of humanization assay for single histone variant swaps. Histone variants are color-coded as in (A). Open dashed-line circles indicate failure to isolate true humanized clones as assessed by PCR genotyping (see Figure S1).

(E) Humanization assays of *Hs*H3.4 and *Hs*H3.5 with nucleosome-stabilizing mutations and H3.5 with added lysine residues. Amino acid alignments shown above. Statistical significance of the mean difference in 5-FOA^R frequency was determined with a 1-way ANOVA test and corrected for multiple comparisons with hypothesis testing (Šídák).

variant, Hho1, which plays specific roles in the compaction of chromatin during sporulation.[13–15]

Histone variant incorporation into chromatin serves as an additional layer of regulation of chromatin structure and function.[7] For example, the variant macroH2A1 encodes a C-terminal macro domain approximately twice the size of its histone fold domain (HFD).[16] *In vitro* the macroH2A1 histone fold preferentially makes heterotypic nucleosomes with replicative H2A and resists chromatin remodeling by reducing the recruitment of the ATP-dependent chromatin remodeler SWI/SNF.[17,18] Additionally, macroH2A1 is enriched at transcriptionally silenced chromatin, directly inhibiting the recruitment of RNA polymerase II, chromatin remodelers, and transcription factors.[6,19,20]

Nucleosomes are organized into phased arrays with a characteristic spacing called the nucleosome repeat length (NRL).[21,22] Nucleosome phasing is typically set against genomic barriers nearest to TSSs, defined by an NDR, and the precise positioning of the first downstream nucleosome (NDR +1 nucleosome) is critical in transcriptional regulation.[23] The complete nucleosome landscape is set by many interacting protein complexes and underlying DNA sequence/mechanics.[24,25] In yeasts, the phased landscape near the TSS is largely determined by the action of ATP-dependent chromatin remodelers, which counteract nucleosome-disruptive processes such as transcription, DNA replication, and repair.[22,24] The combined action of RSC and INO80 remodelers precisely set the +1-nucleosome positioning in yeasts, establishing spacing near genomic barriers such as Reb1 binding sites.[24–26] Internucleosomal distance is independent of nucleosome density both *in vivo* and *in vitro*.[5,27–29] Factors such as IWS1a, ISW1b, or Chd1 further refine nucleosome spacing to the characteristic NRL observed in wild-type (WT) cells.

In vitro chromatin reconstitution using replicative histones has proven to be a powerful probe of structural and functional effects from the bottom up. However, these systems lack cellular processes such as transcription or DNA replication. Remarkably, despite over ~1 billion years of divergent evolution, the replicative histones of yeast can be entirely exchanged with human replicative histones.[5,30,31] These histone humanized yeasts provide a powerful "*in vivo* reconstitution" system of human chromatin, as we can "reset" the composition of DNA packaging in yeast. Here, we have adapted the histone-replacement system to directly test the complementation of replicative histones with the majority of their corresponding variant histones (e.g., does H2A.J substitute for replicative H2A?). We defined a set of human variant histones that can complement their replicative counterparts in yeast (H2A.J, TsH2B, and H3.5). We then focused on dissecting the incompatibility of the human variant histone macroH2A1.2 with yeast chromatin and systematically determined which residues are inviable in yeast. Doing so allowed us to decouple the separate effects of the macro domain and HFD, the latter sufficient for the incompatibility with yeast chromatin. Using both micrococcal nuclease sequencing (MNase-seq) and HiC assays, we show that humanized yeast in which yeast-compatible versions of macroH2A1.2 replace replicative human H2A exhibit surprising structural and functional alterations to their chromatin alongside enhanced genome instability. Thus, while yeast may have never before packaged their genomes with these particular variant histones, it serves as a powerful system to study the impact of chromatin from divergent species.[32]

RESULTS

Humanization of yeast chromatin with non-replicative human histone variants

Yeast can use either the human replicative histones *Hs*H3.1 or the variant *Hs*H3.3,[5,33] with a preference for *Hs*H3.1[5] (for clarity, replicative human histones are explicitly written with a preceding "*Hs*" and yeast histones with a preceding "*Sc*"). However, whether yeast can use other human variant histones is not known. To address this, we adapted our dual-plasmid histone shuffling method to exchange replicative histones for variant histones in yeast (Figure 1B).[5,30,31]

Here, a single replicative human histone gene is replaced by a variant type, and a complementation test is done using our histone shuffle yeast (Figure 1B). We failed to isolate humanized clones for the majority of the histone variants (H2A.Z2, H2A.Bbd, macroH2A1.2, macroH2A2, H3.4, H2B.W), consistent with the idea these histone variants lack essential functions, typically executed by replicative histones, needed for packaging DNA. For example, macroH2A1.2 produced a single clone that appeared after 2 weeks of growth; however, genotyping revealed it still contained yeast histone genes (Figure S1). In contrast, we readily isolated true histone humanized clones for variants *Hs*H2A.J (71% identical [amino acid sequence identity] to yeast H2A), *Hs*TsH2B (63% identical to yeast H2B), and *Hs*H3.5 (86% identical to yeast H3; Figures 1C, 1D, and S1). As these variants complemented their replicative counterparts individually, we tested whether all three together could simultaneously replace replicative H3, H2A, and H2B. Remarkably, *Hs*H3.5, *Hs*H2A.J, and *Hs*TsH2B simultaneously replaced replicative H3, H2A, and H2B, respectively (Figures S1B and S1C). These data suggest that *Hs*H2A.J, *Hs*TsH2B, and *Hs*H3.5, the latter two of which are testis specific,[34,35] retain the essential functions of yeast replicative histones.

Nucleosome stabilizing mutations improve complementation with variants *Hs*H3.4 and *Hs*H3.5

We were curious why certain histone variants failed to complement their canonical counterparts. We first investigated the variant *Hs*H3.5, which humanized less frequently than replicative *Hs*H3.1, and variant *Hs*H3.4 (*Hs*H3T), which failed to humanize altogether (Figure 1D). *Hs*H3.5 and *Hs*H3.4 form unstable nucleosomes *in vitro,* and in both cases, increased instability is attributable to changes to a single amino acid.[34,36] The replicative HsH3.1 residues, known to act as nucleosome stabilizing mutations, were introduced into *Hs*H3.5 (L103F) and *Hs*H3.4 (V111A) and tested for complementation. The stabilizing mutations improved humanization of both variants, with *Hs*H3.4^{V111A} now able to complement *Hs*H3.1 and *Hs*H3.5^{L103F} complementation improved by >100-fold (compared to WT *Hs*H3.5), although each still performed worse than replicative *Hs*H3.1 (Figure 1E). Also, HsH3.5 lacks two conserved lysine residues, K36 and K79, modified by lysine methyltransferases Set2 and Dot1, respectively. Introduction of the two lysine residues into *Hs*H3.5 improved humanization by ~27-fold (in the absence of the stabilizing L103F mutation), suggesting that, in addition to improving nucleosome stability, restoring the two modifiable lysine residues of histone *Hs*H3.5 is critical for proper histone H3 function in yeast.

Human macroH2A1 is a dominant-negative histone variant in *S. cerevisiae*

We next investigated the inability of macroH2A1.2 to replace replicative *Hs*H2A, which could result from its toxicity or lack of essential H2A functions. We confirmed that macroH2A1.2 is expressed in WT yeast from the native *HTA1* promoter and observed correct localization to the nucleus (Figures 2A and

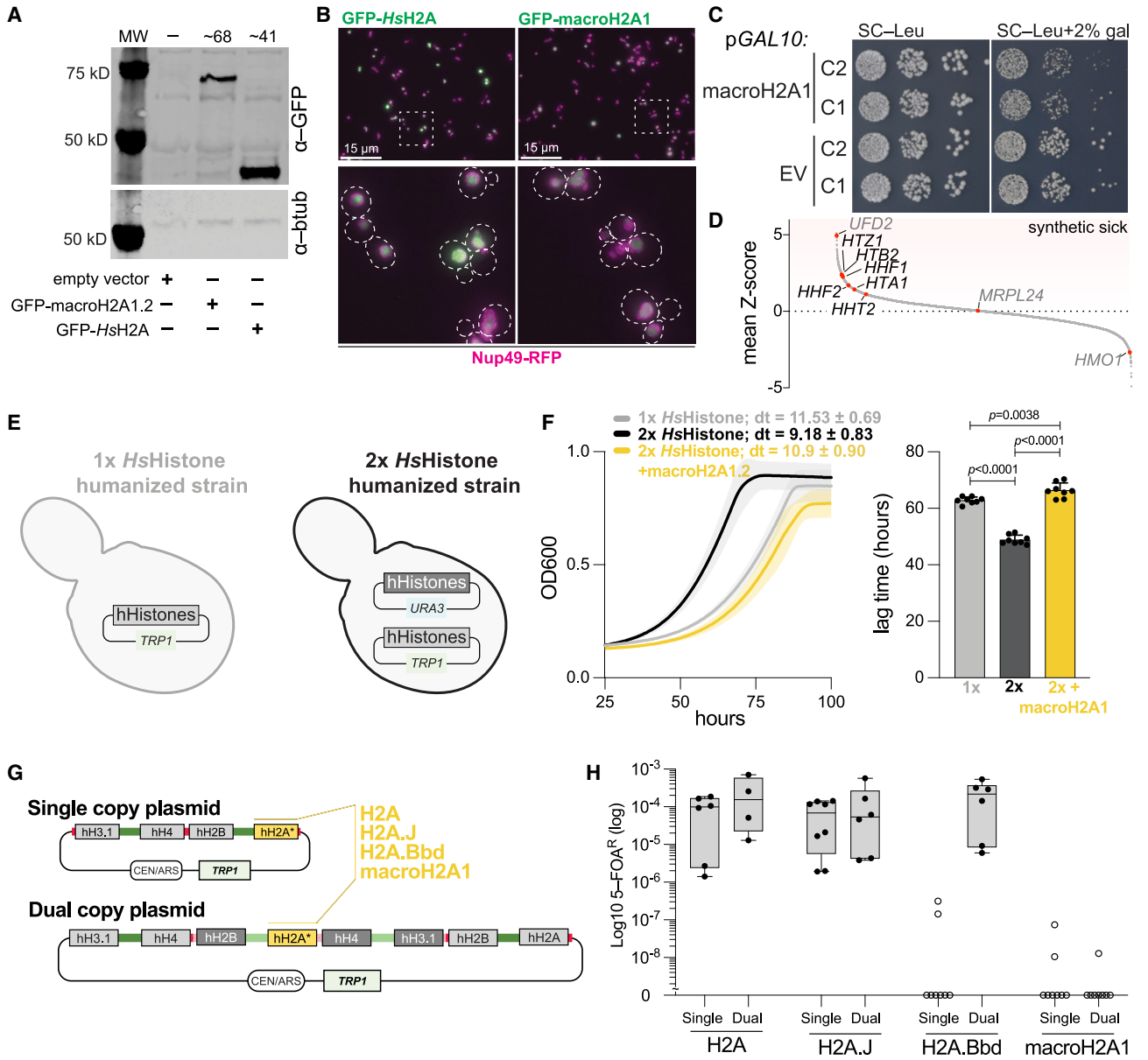

Figure 2. macroH2A1 is a dominant-negative histone variant in yeast

(A) Western blot analysis of histone expression in WT cells.

(B) GFP-macroH2A1 correctly localized to the nucleus in WT cells. Cells with a red fluorescent protein (RFP)-tagged nuclear envelope protein (Nup49-RFP) were transformed with GFP-H2A fusions as labeled and imaged from mid-log phase cultures.

(C) Overexpression of macroH2A1 in WT cells is toxic. Cells with the indicated plasmid (EV, empty vector) were grown in glucose (no expression) or galactose (overexpression).

(D) GIs (genetic interactions) screen of non-essential gene deletions with macroH2A1 overexpression. Histone genes are highlighted, as are 3 example genes that showed negative, no, and positive GIs with macroH2A1 overexpression.

(E) Schematic of strains used in growth assays. The 1× histone humanized strain has a single copy of each human replicative histone on a *TRP1* CEN/ARS plasmid (pDT109). The 2× histone humanized strain has 2 sets of human histones genes on 2 CEN/ARS plasmids with all replicative (pDT109 + pMAH022) or with 1 non-replicate variant (see Table S1)).

(F) Co-expression of macroH2A1 is toxic in histone humanized cells. Growth assays of 1× (gray) and 2× histone humanized yeast (with replicative *Hs*H2A only (black; pDT109 + pMAH022) or replicative *Hs*H2A with macroH2A1(yellow; pDT109 + pMAH87). Left: A_{600} growth curves. Right: calculated lag times. Strains were grown in SC-Trp-Ura medium at 30°C. Statistical significance in the mean change in lag time was determined with a 1-way ANOVA test and corrected for multiple comparisons with hypothesis testing (Šídák).

(legend continued on next page)

2B). Inducible overexpression of macroH2A1.2 resulted in a noticeable growth defect in WT yeasts (Figure 2C). To further understand macroH2A1.2 toxicity, we performed a genome-wide deletion screen of the non-essential yeast genes to explore genetic interactions (GIs) with macroH2A1.2 overexpression (Figure S2A). We identified numerous synthetic sick GIs (*Z* score normalized >2; Table S2) enriched in Gene Ontology (GO) cellular components such as the COMA complex (*MCM21* and *CTF19*), kinetochore (*IML3*, *PAT1*, *MCM21*, *SLX8*, *MCM22*, *CTF3*, *CTF19*), nucleosome (*HTB2*, *HHF1*, *HTZ1*), and organellar large ribosomal subunit (*MRPL36*, *MHR1*, *MRP49*, *MRPL20*, *MRPL10*). Additionally, positive GIs or "suppressors of macroH2A1 overexpression" were enriched for genes within molecular complexes such as transcription elongation factors (*DST1*, *SPT4*), Bfa1-Bub2 complex (*BFA1*, *BUB2*), ribosome (*RPS11A*, *RPS6A*, *IMG1*, *MRP10*, *CBS2*, *RPS27B*, *RPS29A*, *RPS10A*, *MRP7*, *MRPL10*, *RPS19B*), and mitochondrial ATP synthase complex (*ATP1*, *ATP2*; Table S2). These data suggest that macroH2A1.2 interferes with various processes, such as centromere-kinetochore function and the metabolism of mitochondria and ribosomes (Figure S2B). Furthermore, some of the top synthetic sick hits corresponded to the genes encoding yeast histones (Figures 2D and S3C), suggesting that reduced dosage of the native yeast histones exacerbates the toxic effects of macroH2A1.2 in WT yeast. The toxicity of macroH2A1.2 was not rescued by the deletion of yeast's native H2A.Z remodeler, Swr1, but was rescued by the introduction of two mutations (I100T and S102P) in the C-terminal region of macroH2A1.2's HFD, predicted to disrupt H2A's chromatin association[37] (Figures S3A–S3D).

Next, we verified macroH2A1.2 toxicity in the human chromatin background (Figure 2E). As we could not generate macroH2A1.2 humanized yeasts directly, we transformed a histone humanized strain (with all four replicative human histones encoded on a *TRP1* CEN/ARS plasmid) with a *URA3* CEN/ARS plasmid encoding either all four replicative human histones or three replicative human histones plus a single variant histone (e.g., macroH2A1.2). We assayed growth using a high-throughput plate reader and found that the strain with two plasmids encoding only replicative human histones (2× hHistones; doubling time of 9.18 ± 0.83 h and a lag time of 48 ± 1.6 h) grew significantly better than the parental strain with a single plasmid (1× hHistones; doubling time of 11.53 ± 0.69 h and a lag time of 62 ± 1.2 h; Figure 2F). In contrast, co-expression of macroH2A1.2 in the 2x hHistone strain slowed its doubling time to 10.9 ± 0.90 h and increased the lag time to 66.4 ± 2.6 h (Figure 2F). Critically, this was not due to a gene dosage effect of *Hs*H2A, as the 2× hHistone strain with a single *Hs*H2A gene grew normally (Figure S3E). We cannot rule out the possibility that the incoming *URA3* plasmid, encoding macroH2A1.2, was not kept at a copy number similar to that of the *TRP1* plasmid during the experiment. Indeed, passaging these transformants for two cycles invariably led to the loss of the macroH2A1.2 gene, indicating that loss of macroH2A1.2 is positively selected for (Figure S3F).

To avoid loss of the variant histone, we placed the replicative and non-replicative variant histones on the same plasmid (dual-copy histone shuffle, Figure 2G). The dual-copy histone shuffle strain has two advantages: (1) after shuffling, it is more fit as it has two sets of each human histone gene, and (2) it allows the incorporation of variant histones while maintaining an equal copy number between the replicative and variant histones. We tested all histone variants in this system (Figures S4G and S4H), but for simplicity, we describe only the results for three H2A variants—H2A.J, H2A.Bbd, and macroH2A1.2—with the latter two being inviable in the 1:1 replacement of replicative H2A (Figure 1D). When we humanized H2A.Bbd in the presence of replicative *Hs*H2A, we observed robust isolation of humanized colonies (Figures 2H and S4H), suggesting that H2A.Bbd is either not incorporated into chromatin or lacks essential nucleosome functions in yeast. However, we again failed to isolate colonies when attempting to humanize macroH2A1.2 in the presence of replicative HsH2A (Figures 2C–2H and S4H). Combining the conversion to human chromatin and expression of macroH2A1.2 may synergistically lead to loss of viability, contrasting the prior experiments (overexpression in WT cells or transformation of already humanized yeast), which only tested the expression of macroH2A1.2 in the yeast or human chromatin environments. Collectively, these data suggest that macroH2A1.2 is toxic once incorporated into the chromatin of *S. cerevisiae*.

Both the macro and HFDs of macroH2A1.2 negatively affect yeast viability

Amino acid swaps between related histones, such as *Drosophila* H2A and H2A.Z,[38] or between human and yeast replicative histones,[5] is a powerful approach to dissecting functional differences. We reasoned that the same approach could be used between replicative human H2A and human macroH2A1.2. We performed these experiments using the single-copy plasmid system with replicative *Hs*H2A replaced with macroH2A1.2 mutants or chimeric constructs. We observed that a chimeric construct with the macro domain of macroH2A1.2 grafted to replicative *Hs*H2A resulted in the isolation of histone humanized yeast at a significantly reduced frequency from replicative *Hs*H2A (~362-fold reduction). We called these strains "H2Amacro1.2" (color-coded yellow in Figure 3A).

We could not, however, isolate histone humanized yeast with only the HFD of macroH2A1.2 alone (Figure 3A). To fine-map the inviable residues of macroH2A1.2 HFD, we attempted to humanize (1) only the HFD of macroH2A1 (macroH2A1-HF) or (2) chimeric fusions of macroH2A1-HF with *Hs*H2A (replacing the N- or C-terminal tails of replicative *Hs*H2A with corresponding regions of macroH2A1-HF; Figures 3A and S7A). We determined that the C-terminal region of macroH2A1-HF (replacing *Hs*H2A C termini) was sufficient to block histone humanization (Figures

(G) Diagram of single-copy (pDT109) and dual-copy (pMAH342) human histone expression vectors. H2A variants can be cloned into the site colored yellow (pMAH345). Promoters are from the native histone cluster loci, dark green *HTA1B1* and *HHF2T2*; light green *HTA2B2* and *HHF1T1*. The yeast histones are derived from the histone loci of *S. eubayanus* and are encoded on the Superloser plasmid (Figure S4; pMAH316).
(H) Quantification of humanization rates for the various human variant histones in either the absence (single) or presence (dual) of a second set of replicative human histones.

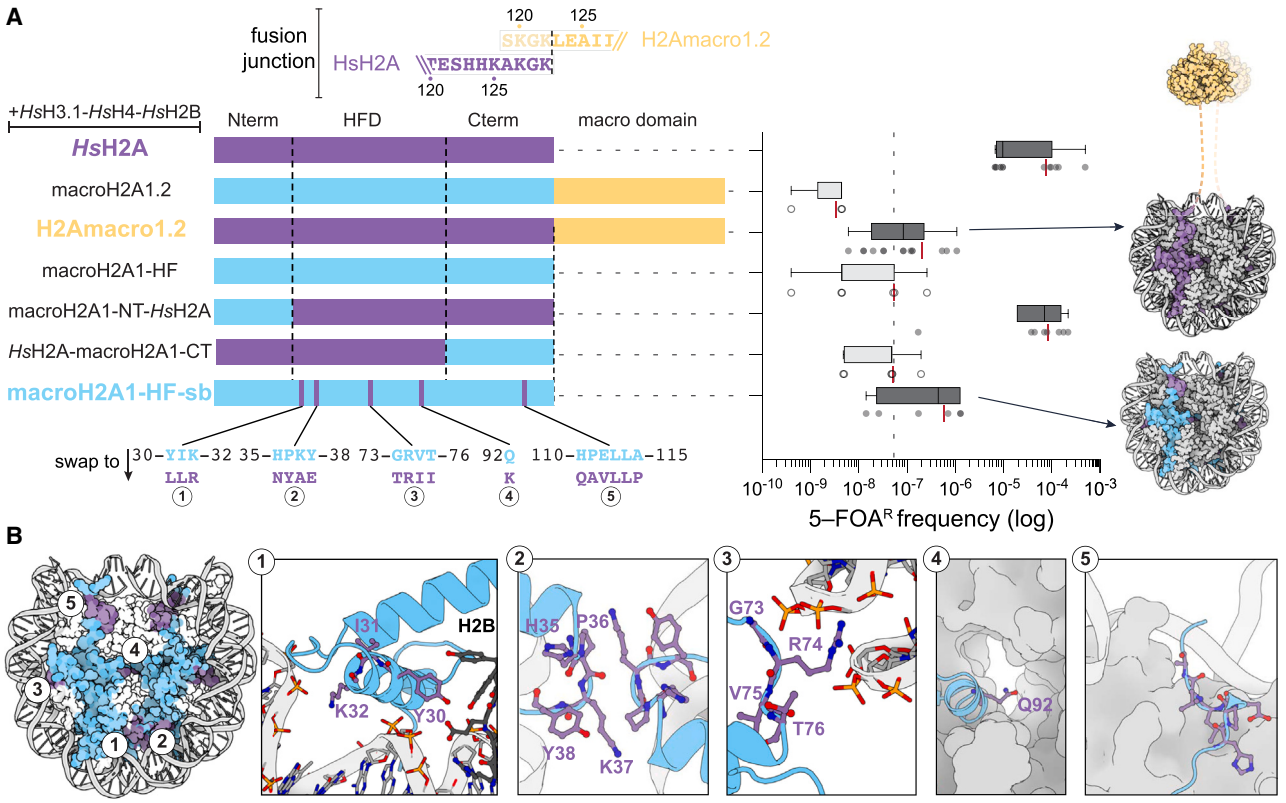

Figure 3. Contributions of the macro and HFDs to the inviability macroH2A1.2

(A) Humanization of yeast with macroH2A1 chromatin. Right: diagrams of replicative *Hs*H2A-macroH2A1 chimeras. Details of macroH2A1 histone fold swap-back experiments are found in Figure S5. Above is a diagram showing the precise fusion junction used in the *Hs*H2A-macro1.2 fusion. Left: quantification for the humanization assay of replicative *Hs*H2A, macroH2A1, and the chimeras. The swap-back details are displayed below the macroH2A1-HF-sb construct. Open circles indicate that the 5-FOA^R colonies isolated retained the yeast histones. Boxes represent the median with 25th to 75th percentiles, with whiskers extending to the 5th to 95th percentiles. Dots underneath represent each replicate, with red lines representing the mean 5-FOA^R frequency. Dashed line at ~10^{-7} represents the average background frequency of isolating spontaneous *ura3* mutants in our shuffle assay. To the right are illustrations of the H2Amacro1 (macro domain is fused to *Hs*H2A) and the macroH2A1-HF-sb constructs.

(B) View of the human macroH2A1 nucleosome (PDB: 1U35) with swapped residues highlighted in purple. Enlarged views showing the details of the swap-back residues; note that the native macroH2A1 residues are shown; numbering corresponds to macroH2A1. Collectively, the inviable residues are either involved in interactions between the H2A-H2B dimers (Tyr38), between H2A and the DNA phosphate backbone (Lys32 and Arg74), the docking domain (Gln92), and near the DNA entry/exit site (residues 110–115), suggesting that mutating these residues to the corresponding H2A residue helps to overcome the increased stability of macroH2A1 nucleosomes.[39]

3A and S7A). In contrast, the N-terminal tail of macroH2A1-HF functionally replaced the N-terminal tail of *Hs*H2A (Figures 3A and S7A). To narrow down specific incompatible residues, we performed extensive amino acid swap experiments of macroH2A1-HF (STAR Methods; Figures S5B–S5J), identifying a minimal set of 18 residues in the HFD and C terminus of macroH2A1 that when swapped to the corresponding *Hs*H2A residues led to isolation of bona fide macroH2A1 HFD humanized yeast. We refer to these strains as "macroH2A1-HF-sb" ("sb": swap-back, color-coded light blue in Figures 3A, 3B, and S7J).

macroH2A1-HF-sb and H2Amacro1 humanized yeasts have reduced fitness

MacroH2A1-HF-sb and H2Amacro1.2 humanized yeasts formed large cells with markedly slow growth rates (Figures S6A–S6F). We observed a cell cross-sectional area on average 4.2 times larger than WT yeast (*Sc* histones; Figures S6A and S6B; average cross-sectional area of 13 μm^2 versus 6.3 μm^2). We observed an increase in doubling time to over >15 h in macroH2A1-HF-sb and H2Amacro1.2 humanized yeasts (Figures S6C and S6D). Relative to WT yeast, this represents an increased doubling time of 4.3-fold and 5.1-fold for macroH2A1-HF-sb and H2Amacro1 humanized yeasts, respectively. In comparison, histone humanized yeasts with *Hs*H2A displayed an increased doubling time of 2.4-fold relative to WT yeast. Furthermore, macroH2A1-HF-sb and H2Amacro1 humanized yeasts spend a considerably longer time in the lag phase, on average ~60 h versus 8.2 h and 39.5 h for WT yeasts and histone humanized yeasts with *Hs*H2A, respectively (Figure S6E).

We continually passaged the macroH2A1-HF-sb and H2Amacro1 humanized yeasts-rich medium for up to 60 generations—over 4 months—to select for improved growth rates. In these

evolved strains, we observed modest improvement in growth rate (Figures S6D and S6F), as doubling times improved by ~0.18-fold and ~0.33-fold for macroH2A1-HF-sb and H2Amacro1.2 humanized yeasts, respectively, although the variance in doubling times was reduced (Figure S6F). The time spent in lag phase was marginally improved by ~0.24-fold and ~0.15-fold for macroH2A1-HF-sb and H2Amacro1 humanized yeasts, respectively (Figure S6E). Therefore, continuous passaging led to small but significant improvements to growth in both macroH2A1-HF-sb and H2Amacro1.2 humanized yeasts.

We performed whole-genome sequencing on the ancestral and evolved clones to identify mutations associated with the fitness increase (Table S3). Surprisingly, we detected a notable mutation in the HFD of the *Hs*H2A domain (R35I) in the H2Amacro1.2 strains. This residue interacts with the DNA phosphate backbone, and it is, coincidentally, the orthologous residue of macroH2A1-HF that, when swapped to the replicative HsH2A residue, was found to improve humanization (K32R; Figure S5G; see STAR Methods). Additionally, we identified a large deletion of the nonessential histone H2B amino-tail (H2BdelG13-K24) in macroH2A1-HF-sb humanized yeast. Deletion of histone H2B amino-tail *in vitro* destabilizes nucleosomes in a thermal stability assay,[40] suggesting, alongside the observed *Hs*H2A-R35I mutation, that one route by which yeast adapt to macroH2A1 HFD or macro domain is through nucleosome destabilizing mutations.

Overall, we identified 52 mutations, 42 of which were nonsynonymous mutations and most of which were not in the histone genes (Table S3). Next, we constructed an interaction network from the nonsynonymous mutations using the string algorithm (Figure S6G). The core of this interaction network (cluster 3; orange) was enriched in chromatin-based biological processes such as histone lysine demethylation (false discovery rate [FDR] = 0.0033) and chromatin assembly or disassembly (FDR = 4.37e−5). Additionally, we saw an enrichment for cellular components such as cytosolic ribosome (cluster 4; yellow, FDR = 0.00032) and biological processes such as endocytosis (cluster 2; red, FDR = 0.00036) and ubiquitin-mediated proteolysis (cluster 5; green, FDR = 0.0200). These analyses indicate that both macroH2A1-HF-sb and H2Amacro1.2 evolved through the selection of mutants from a non-random set of genes, which are likely to be adaptive. However, as all clones were isolated in the background of the *DAD1*^{E50D} mutation, a mutant that we have shown to be a potent suppressor of histone humanization,[5,31] we cannot rule out the possibility of pleiotropy or dependencies of these mutations on *DAD1*^{E50D}; therefore, we proceeded by studying the ancestral strains that exhibited the fewest mutations relative to the parental strain (Table S3).

The histone fold and macro domain of macroH2A1.2 increase NRL in yeast

To assess changes to chromatin structure in humanized yeast, we performed MNase digestions on cross-linked chromatin isolated from strains with yeast histones (*Sc*; WT), histone humanized yeast with replicative *Hs*H2A and the histone humanized yeast with either macroH2A1-HF-sb or H2Amacro1.2. Analysis of the digest on an agarose gel revealed that replicative histones (either *Sc* or *Hs*H2A), regardless of species, formed correctly phased nucleosomes (Figure S7A, *Sc* and *Hs*H2A panels), as previously reported.[5] Closer examination of the digestion product by capillary electrophoresis revealed that the oligonucleosome array lengths were increased in humanized yeast with either macroH2A1-HF-sb or H2Amacro1.2 (Figures 4A, S9A, and S9B). From the slope of these increments, we estimated a statistically significant increase in the NRL by 10–14 bp in humanized yeast with either macroH2A1-HF-sb or H2Amacro1.2 (Figure 4A; Table S3). Fragment lengths from *Hs*H2A humanized yeast were, on average, ~10 bp larger than the *Sc* control (Figure 4A), and this 10-bp increase was fixed across all oligonucleosome arrays (mono- to penta-nucleosomes), consistent with the idea that replicative human histones more tightly wrap DNA,[41–43] but do not alter the positioning of nucleosomes in yeast.[5] These observations are consistent with and strongly support our direct measurements of nucleosome particle sizes from histone humanized yeast with transmission electron microscopy.[44]

To confirm increased NRL in macroH2A1-HF-sb or H2Amacro1.2 humanized yeast, we sequenced the MNase digested DNA (MNase-seq) and mapped the mono-nucleosome fragments to estimate NRLs relative to TSSs (Figure 4B; see STAR Methods). On average, we mapped the position and occupancies of ~70,000 nucleosomes in each sample (Table S3). Composite-gene analysis of nucleosome occupancies and positions supported the increased NRL relative to the TSS in the humanized yeasts with either macroH2A1-HF-sb or H2Amacro1.2 histones and revealed lower nucleosome occupancies across the gene bodies (Figures 4B, S9C, and S9D). On average, nucleosome occupancy was reduced by ~16% in the H2Amacro1.2 humanized strains and by ~14% in the macroH2A1-HF-sb humanized strains, compared to *Sc* histones (Figure 4C). From our mono-nucleosome maps, we estimated the global NRL by measuring the spacing from the +1 to +5 nucleosomes from genes that displayed well-phased nucleosomes (STAR Methods), observing a net increase of 10–15 bp to the NRLs in humanized yeast with either macroH2A1-HF-sb or H2Amacro1.2 (Figure S7F). As inference of NRL from mono-nucleosome positioning could be influenced by population averages, we also inferred locus-specific NRLs by directly using the di-nucleosome fragment lengths from our MNase-seq data (Figure S7E). In agreement, NRL estimates using di-nucleosome fragments showed increased locus-specific NRL in humanized yeast with either macroH2A1-HF-sb or H2Amacro1.2, with NRL increase being the most extreme in the latter (Figure 4D).

macroH2A1 chromatin is associated with transcriptional dysfunction

We observed an accumulation of nucleosomes in the NDR upstream of the TSS in humanized yeast with either macroH2A1-HF-sb or H2Amacro1.2, prompting us to investigate the transcriptomic effects of these variants (Figures S7G, S7H, and S10A). Differential expression analysis revealed numerous transcriptional changes to the humanized yeasts with either macroH2A1-HF-sb or H2Amacro1 chromatin compared to *Sc* histones (WT; Figure S9A; Table S4). Intriguingly, a transcript's fold change in expression (versus *Sc* histones) was negatively correlated with its abundance in *Sc* histone yeasts (Figure 5A). In other words, the down-regulated genes were biased to genes that are highly expressed in *Sc* histone yeasts and vice versa,

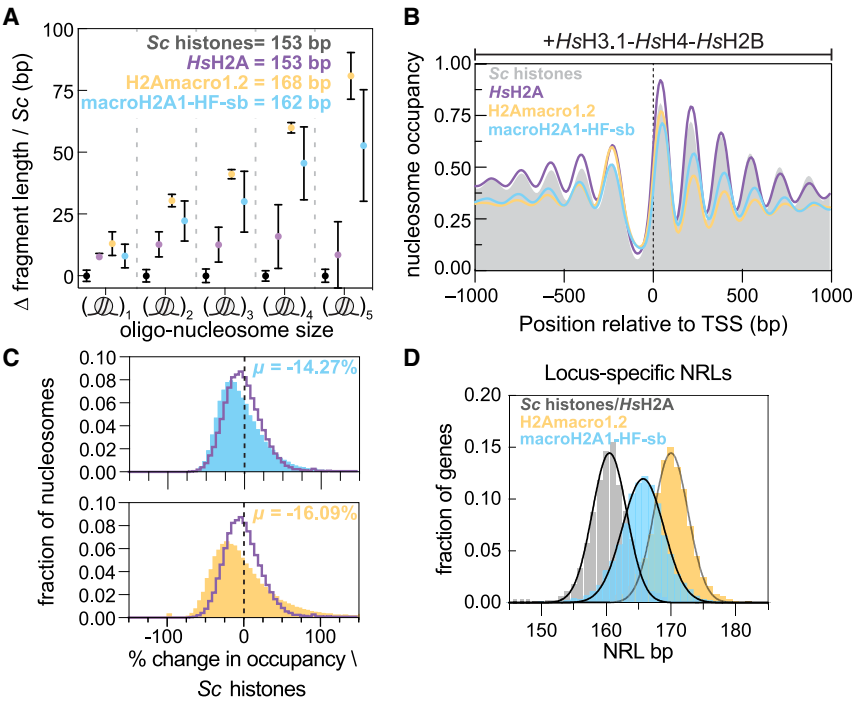

Figure 4. macroH2A1 comprised chromatin has increased NRL

(A) Difference in fragment length compared to WT-digested chromatin. Fragment size analysis of MNase digested DNA using capillary electrophoresis (see Figure S7B). Differences in the average fragment lengths (compared to *Sc* histones) are shown with the SD of 3 biological replicates. Calculated NRLs (based on the slope of the fragment sizes) are shown.

(B) Composite plot of nucleosome occupancy relative to the TSS of 5,206 protein-coding genes (genes with annotated TSS from Park et al.[45]). Gray background occupancy is the mean occupancy of WT yeast, and colored lines are the mean occupancies of the indicated strain.

(C) Change in nucleosome occupancies across the genome. Relative nucleosome occupancies were determined for each humanized strain compared to the *Sc* histones strain, and the distribution in percent change is shown. Data are from the mononucleosome maps in biological triplicate. The distribution of HsH2A humanized strain is shown as an overlayed histogram colored purple. The average change in nucleosome occupancy for *Hs*H2A humanized strain, compared to *Sc* histones strain, was −5.009%.

(D) Locus-specific di-nucleosome length distribution shows increased NRLs in both chimeric *Hs*H2A-macroH2A1.2 constructs (n = 5,801 genes; see STAR Methods). The locus-specific di-nucleosome fragment lengths were determined from 3 biological replicates. Significance in NRLs was determined by a pairwise comparison to WT (*Sc* histones) using a 2-tailed t test of the estimated average NRL of each gene; macroH2A1-HF-sb, $p < 0.0001$; *Hs*H2Amacro1.2, $p < 0.0001$. Fitted Gaussian distributions are plotted with a mean NRL: *Sc* histones and *Hs* histones of 160.5 bp, macroH2A1-HF-sb of 165.7 bp, and *Hs*H2Amacro1.2 of 170.0 bp.

suggesting that the dynamic range in transcript abundance is reduced in histone -humanized yeast with either macroH2A1-HF-sb or H2Amacro1.2. Shared down-regulated genes were enriched in Kyoto Encyclopedia of Genes and Genomes pathways such as ribosome and glycolysis, while the shared up-regulated genes were enriched in biological processes such as flocculation and cell adhesion (Figures S9B and S9C). Most up-regulated genes were enriched in the subtelomeric regions of chromosomes, consistent with the loss of telomere silencing (Figure S9D). Gene set enrichment analysis of H2Amacro1.2- or macroH2A-HF-sb-specific differentially expressed genes (compared to *Sc* histones) revealed numerous differentially expressed pathways (Figures S9E and S9F). For example, macroH2A-HF-sb histone humanized yeast showed up-regulation of genes involved in amino acid (isoleucine, valine, and tryptophan) degradation, whereas H2Amacro1.2 histone humanized yeast showed down-regulation of the same amino acid degradation genes and up-regulation of genes involved in certain amino acid biosynthetic pathways (Figures S9E and S9F).

A composited gene plot of nucleosome occupancies showed that down-regulated genes had higher nucleosome accumulation in the NDR (Figure 5C). However, across all coding genes, the increase of NDR nucleosome occupancy did not correlate with the change of a gene's expression (Figure S8B), suggesting that the accumulation of nucleosomes in the NDR is downstream of the transcriptional effects. Instead, we observed that genes that were highly expressed in WT (*Sc* histones) showed the highest degree of accumulation of nucleosomes in their NDR in humanized yeast with either macroH2A1-HF-sb or H2Amacro1.2 (Figures S8C and S8D). For example, genes in the top 10% of abundance in WT yeasts were significantly down-regulated, whereas those in the bottom 10% showed no change in expression (Figure S8E). Gene set enrichment analysis of the genes in the top 10% group revealed strong enrichment in processes related to translation, such as small and large ribosomal subunit biogenesis (Figure S8F). These results are consistent with our findings that histone humanized yeast's ribosomal RNA levels are reduced.[44]

Lastly, we investigated whether transcriptional changes affected the positioning of nucleosomes in either macroH2A1-HF-sb or H2Amacro1.2 histone humanized yeast. We observed that nucleosomes were shifted downstream of their expected position more dramatically for the down-regulated genes (Figures 5B and 5C). Examination of the relative gene-specific nucleosome positions showed that down-regulated genes had greater increases in their NRLs, as indicated by more extreme shifts in nucleosome positions downstream of the TSS (Figures S10B–S10F). These results indicate that genes with increased expression retain better nucleosome positioning downstream of the TSS.

Specific transcriptomic effects of macroH2A1-HF-sb and H2Amacro1.2 histone humanized yeasts

Next, we considered transcriptomic changes compared to the *Hs*H2A histone humanized yeast (Figure 5D). As both chimeric variants of *Hs*H2A-macroH2A1.2 displayed numerous aneuploid

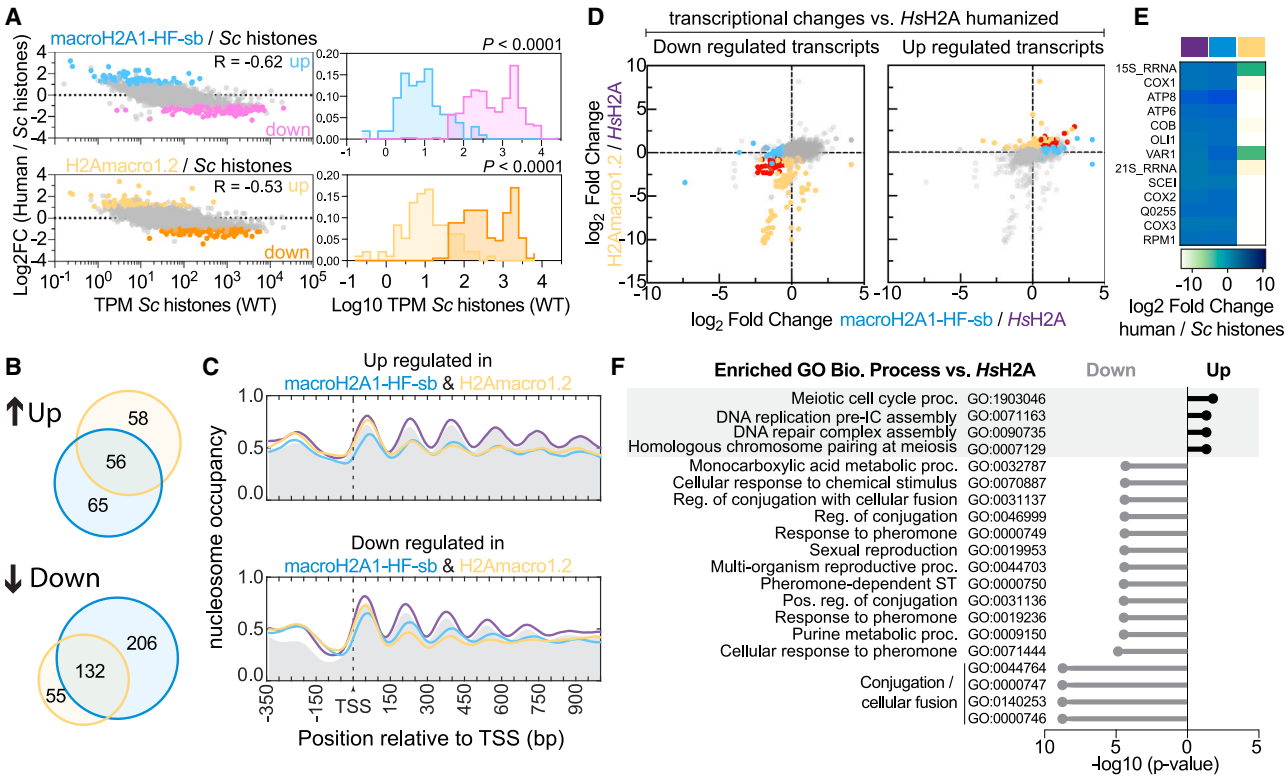

Figure 5. Transcriptional and nucleosome positioning changes in chimeric H2A-macroH2A1.2 histone humanized yeasts

(A) Differentially expressed genes are biased by the transcript's abundance in WT yeasts (*Sc* histones). Log2 fold change (FC) in expression (compared to *Sc* histones) is plotted against WT transcript abundance (transcripts per million; TPM). Spearman correlation between log2FC and WT TPM is shown for each strain. To the right are histograms of the WT TPM split by down- and up-regulated genes for the given strain (log2FC > 1 and <−1, FDR adjusted $p < 0.01$). The difference in mean WT TPM of each group is compared (Kolmogorov-Smirnov test).

(B) Venn diagrams of differentially expressed genes in chimeric H2A-macroH2A1.2 histone humanized yeasts compared to WT yeasts; top, up-regulated; bottom, down-regulated.

(C) Up-regulated genes in chimeric H2A-macroH2A1.2 histone humanized yeasts exhibited better nucleosome positioning than down-regulated genes. Shown are composite-gene nucleosome positioning and occupancy plots near the TSS. Averages are colored by strain: WT (*Sc* histones), gray background; HsH2A, purple; macroH2A1-HF-sb, blue; H2Amacro1.2, yellow.

(D) Differentially expressed transcripts in macroH2A1-HF-sb and H2Amacro1.2 histone humanized yeasts compared to *Hs*H2A histone humanized yeasts. Log2FC values of each transcript are plotted against each other; red, differential expression is shared between macroH2A1-HF-sb and H2Amacro1.2; yellow, differential expressed in H2Amacro1.2; blue, differential expressed in macroH2A1-HF-sb (log2FC > 1 and <−1, FDR adjusted $p < 0.01$).

(E) Loss of mitochondrial DNA is evident from transcriptome analysis in H2Amacro1.2 histone humanized yeasts. Shown is a heatmap of mitochondrial-encoded genes and their log2FC in expression when compared to WT (*Sc* histones).

(F) Enriched GO biological processes of shared up- and down-regulated genes in chimeric H2A-macroH2A1.2 histone humanized yeasts (compared to *Hs*H2A histone humanized yeast).

chromosomes (discussed below), we examined the effect of aneuploidy on the transcriptome. We observed that the level of aneuploidy correlated one-to-one with the observed median transcript abundance of the chromosome presenting aneuploidy, suggesting that transcription is not compensated by the presence of aneuploid chromosomes (Figure S11A). RNA-seq showed a loss of transcripts from mitochondrially encoded genes, confirming the loss of mitochondria in H2Amacro1.2 histone humanized yeast (Figure 5E). A gene set enrichment analysis of the shared up- and down-regulated genes (versus *Hs*H2A) revealed an unexpected up-regulation of genes involved in meiotic cell progression (*CLB6*, *CSM2*, *HED1*, *HOP1*, *MEI5*, *OSW1*, *SPO19*, *SPO21*, *SPO75*, *SPR28*, *SPS22*, *ZIP1*, *ZIP2*) and a down-regulation of genes involved in processes related to cell mating and pheromone response (*FUS3*, *KAR4*, *GET3*, MF(ALPHA)2, *GPA1*, *STE12*, *BAR1*, *FAR1*, *SAG1*, *STE3*, *MFA2*, *AGA1*, MF(ALPHA)1; Figures 5F and S6I–S6K). This is consistent with a reduced competency to mate in a mating-type assay (Figure S6H). Lastly, examination of macroH2A1-HF-sb-specific or H2Amacro1.2-specific differentially expressed genes revealed numerous biological processes enriched to either lineage (Figures S11B–S11K).

macroH2A1 histone fold and macro domains alter three-dimensional (3D) genome organization and drive genome instability

Given the effects on the chromatin fiber at short scales (NRL), we investigated how chromatinization with either macroH2A1-HF-sb

or H2Amacro1.2 affects genome structure and stability. We first explored the consequences of chromatin folding by performing Hi-C. Consistent with our companion paper,[44] we observed a reduction in inter-pericentromeric contacts in histone humanized yeast, evident by the loss of the typical cruciform arrangement near the pericentromere (Figures 6A, 6B, and S12B). Consequently, we also observed increased intra-contracts between chromosomal arms, as indicated by the ratio maps (Figures 6C and 6D). These alterations were consistently more pronounced in chimeric *Hs*H2A-macroH2A1.2 humanized yeasts than in the humanized *Hs*H2A counterpart (Figures 6B, 6C, S12A, and S12B). Quantification of inter-pericentromeric contacts confirmed a significant decrease in the chimeric *Hs*H2A-macroH2A1.2 humanized yeast, suggesting structural changes in the pericentromeric chromatin and strong centromere de-clustering (Figures 6E and S12B). This is supported by our observations of elevated levels of centromeric RNA in all humanized strains, particularly in those with macroH2A1-HF-sb or H2Amacro1.2 histones (Figure S12C). We observed high chromosome instability (CIN) levels in the chimeric *Hs*H2A-macroH2A1.2 humanized yeasts, as all strains had one or more aneuploid chromosomes (Figures 6F and S13; Table S3).

Chromatinization with either macroH2A1-HF-sb or H2Amacro1.2 decreased short-range intra-chromosomal contacts (<20 kb; Figures 6B–6D and S12A). This effect was not observed in the *Hs*H2A humanized yeast, suggesting that it is a consequence of the changes to chromatin folding in the macroH2A1-HF-sb and H2Amacro1.2 humanized yeasts. Loss of short-range intra-chromosomal contacts may result from the reduced nucleosome occupancy in the chimeric *Hs*H2A-macroH2A1.2 humanized yeasts (Figure 4A). Increases in the NRL may facilitate chromatin fiber flexibility, potentially leading to chromatin decompaction.[46,47] Correspondingly, the loss of short-range intra-chromosomal contacts is accompanied by an increase in long-range intra-chromosomal contacts (>20 kb) in both macroH2A1-HF-sb and H2Amacro1.2 humanized yeasts (Figures 6B–6D and S12A). Increased distal interactions are partly attributable to the loss of strong inter-pericentromeric interactions (as mentioned above), which typically constrain chromosomes. We propose that the combination of decreased nucleosome occupancy and increased nucleosome linker length drive an overall decompaction of chromatin at the short scale, biasing an apparent increase in long-range interactions.

Ectopic chromosomal rearrangements in macroH2A1-HF-sb and H2Amacro1.2 humanized yeasts

Examination of our whole-genome sequencing data revealed how genomes evolved in the presence of macroH2A1-HF-sb and H2Amacro1.2 chromatin. In all clones, multiple chromosomal rearrangements were observed (Figures 7, S12D–S12F, and S13A–S13D). These were less frequent in the H2Amacro1.2 humanized yeasts (Figures S12D and S12F). For example, we observed in H2Amacro1.2 humanized yeasts an aneuploid chromosome *XII* in which 1 copy displayed an internal deletion of ~160 kb, with the breakpoints mapping near two Ty1 long terminal repeats (LTRs; Figures S12G and S12H). Intriguingly, the chromosome *XII* aneuploidy and the internal deletion were stable across the 60 generations we tracked (Figures S12D and S12F).

In contrast, examination of whole-genome sequencing coverage plots from clones 1 and 4 of the macroH2A1-HF-sb humanized yeast revealed many chromosome breakpoints, as indicated by abrupt changes in sequence depth (Figures S13A–S13D). Both clones were polyploid, with the majority of chromosomes at a copy number of two (normalized to regions of deletions that contain essential genes). Many breakpoints mapped to repetitive elements such as Ty elements, Ty LTRs, tRNAs, and sub-telomeres. Therefore, we could not conclusively map these putative chromosomal rearrangements using short paired-end Illumina sequencing data. As we performed our Hi-C experiments in the ancestral strains that did not exhibit these putative chromosomal rearrangements (Figures S13A–S13D), we could not leverage the contact maps to map them.

Therefore, we generated nanopore reads from three isolates from clones 1 and 4 of macroH2A1-HF-sb humanized yeasts. We observed numerous translocations between Ty, LTRs, tRNAs, and sub-telomeric regions (Figures 7A and 7B; Table S5). For example, we observed a large ~43 kb internal deletion on chromosome V between the Ty1 elements YERCTy1-1 and YERCTy1-2 (Figure S13E). Additionally, we observed a well-supported translocation between chromosomes *XIV* and *XVI*, which we mapped to a translocation event between two isoleucine tRNAs (Figures 7C and S13F). In conclusion, long-read sequencing revealed the complex nature of chromosomal structural variants in macroH2A1-HF-sb histone humanized yeast.

DISCUSSION

Biochemical reconstitutions have established that ATP-dependent chromatin remodelers set the phasing of nucleosomes.[22,24–27] Our observations that replicative histones, regardless of species, result in normal phasing of nucleosomes in yeast support the idea that replicative nucleosomes' interactions with chromatin remodelers are deeply conserved.[5] In line with this, *in vitro* reconstitutions have also shown that purified yeast chromatin remodelers properly phase replicative histones, regardless of the species' histones examined.[25] However, as our data suggest, certain histone variants may lack (or have new) interactions essential to maintaining correct phasing in yeast. We propose that histone variants may modulate locally distinct nucleosome organization through exclusionary interactions with chromatin remodelers. We do not address this hypothesis directly using our *in vivo* system, as we do not precisely modulate the levels of specific chromatin remodelers. However, biochemical work has shown that macroH2A1 nucleosomes display reduced recruitment of certain chromatin remodelers,[18] and the efficient deposition of macroH2A1 in mammals requires the ATPase-dependent action of LSH/HELLS, an SNF2-like chromatin remodeler.[48] While yeast does encode a homolog of mammalian LSH, Irc5, it likely lacks the specific protein-protein interactions required to interact with macroH2A1.[49] Future efforts should address the effects of histone variant type in combination with chromatin remodelers.

The phasing and occupancy of nucleosomes is critical for genome integrity.[50] We observed increased rates of genome instability brought on by chromatinization with the two macroH2A1 derivatives studied here. For clones with

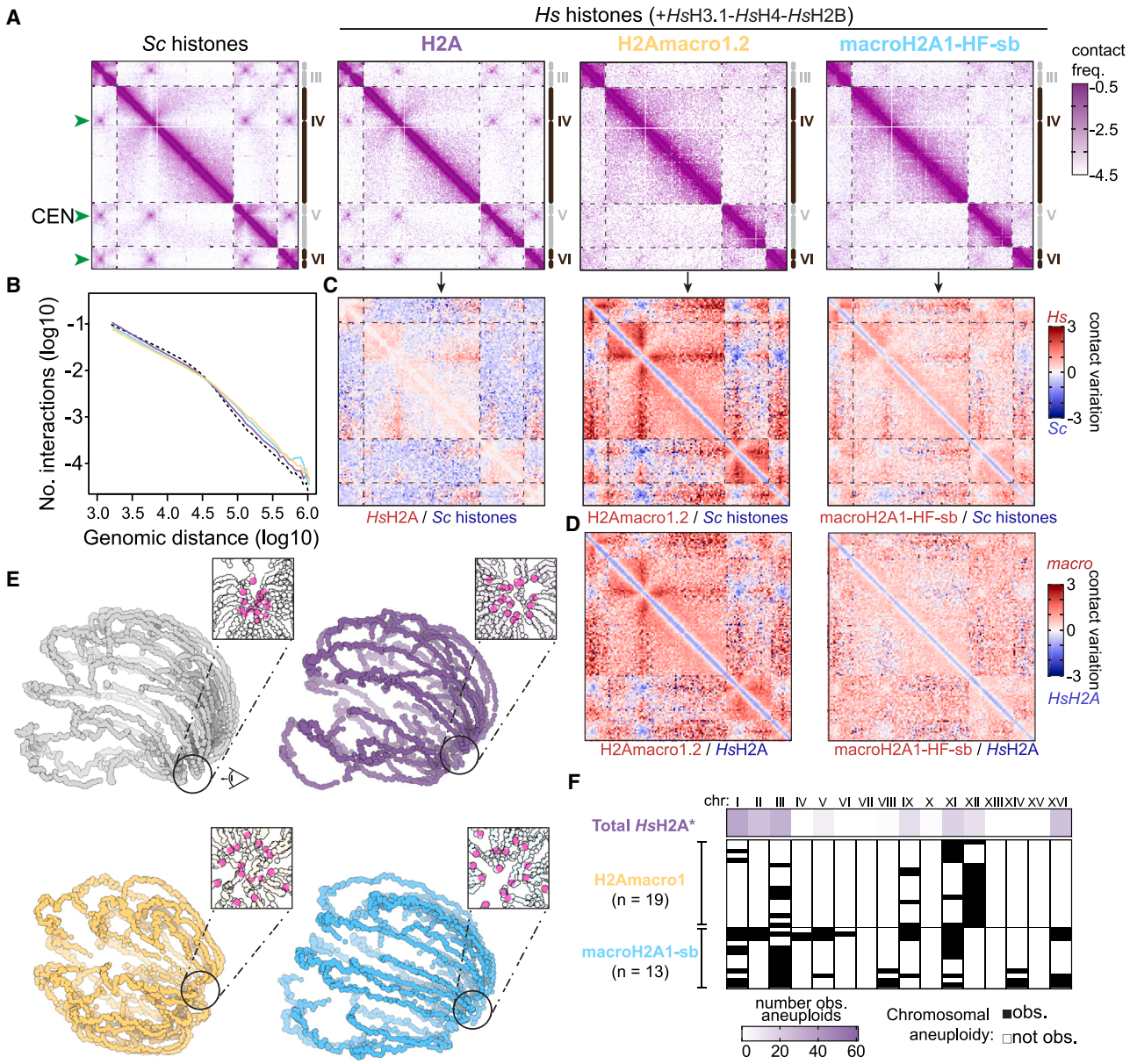

Figure 6. Decreased short-range chromatin interactions and CIN in macroH2A1 humanized yeast

(A) Subset of Hi-C heatmaps showing chromosomes *III*–*VI*. Inter-centromeric contacts are indicated with a green arrow. Normalized contact frequencies were binned at 5-kb resolution. Purple–white color scale indicates increased contact frequency (log10).

(B) Contact probability decay as a function of the genomic distance plot represents the average decay of intra-chromosomal contact frequency with the increment in their genomic distances.

(C) Log2-ratio maps of histone humanized yeast to WT (*Sc* histones) contact maps in (A).

(D) Log2-ratio maps of chimeric H2A-macroH2A1.2 histone humanized yeast to HsH2A histone humanized yeast contact maps in (A).

(E) 3D average representations of the complete Hi-C maps in (A).

(F) Observed chromosomal aneuploidies in macroH2A1 histone humanized yeast. Aneuploidies were inferred from chromosome sequencing coverage (black, observed; white, not observed). Each row represents 1 isolate. Chromosome coverage plots are displayed in Figure S13. The total number of observed aneuploids for each chromosome in *Hs*H2A histone humanized yeasts is shown (n = 61 total strains; data are adapted from previous work[31]). Note that the total number of observed aneuploids is taken from a diverse set of strains, and the isogenic *Hs*H2A histone humanized strain (Dad1^{E50D}) did not display any aneuploids.

H2Amacro1.2, we observed only one large, stable deletion event over many generations. However, for the macroH2A1-HF-sb clones, we observed a continuing accumulation of deletion and rearrangements, suggesting that the HFD of macroH2A1 contributes the most to genome instability. There is substantial evidence of the role of macroH2A1 in maintaining genome stability in metazoans.[48,51] MacroH2A1 histone promotes the resolution of DNA double-strand breaks (DSBs)

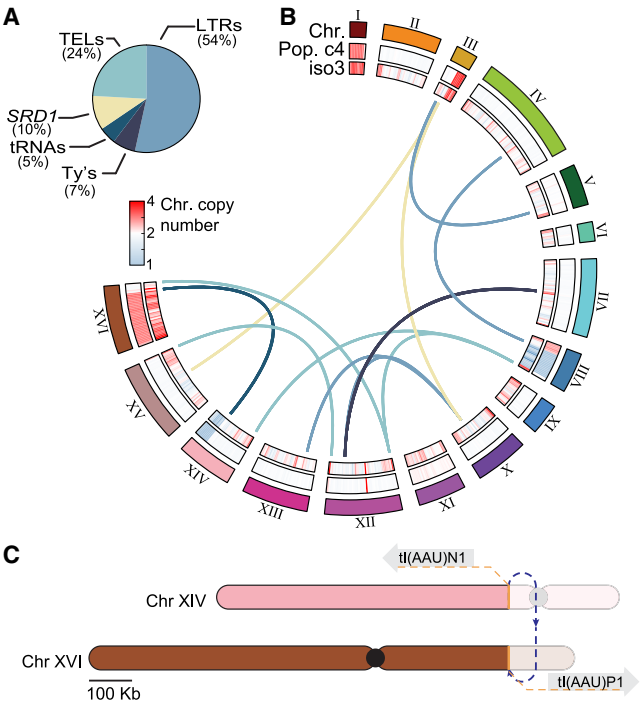

Figure 7. The histone fold of macroH2A1 promotes ectopic recombination events between repetitive elements

(A) Pie chart depicts the relative proportions of each class of repetitive elements for which we observed translocation events between (clones 1 and 4; Table S5).

(B) Circos plot of chromosomal rearrangements inferred from nanopore sequencing of macroH2A1-HF-sb humanized yeast clone 1. Chromosomes are presented in a clockwise fashion from chromosome (Chr.) *I* to chromosome *XVI*. For each chromosome, the sequencing coverage (log2 normalized to the median, binned at 24 kb) is plotted from both the Illumina data (Population Clone4 track [Pop. c4]) and nanopore data (isolate3 track [iso3]). Translocations are plotted as connecting links between chromosomes and are colored by the type of sequences that recombined.

(C) Schematic of the translocation between isoleucine tRNAs on chromosomes *XIV* and *XVI*.

through homologous recombination (HR) by the formation of protective domains of chromatin.[52,53] However, in our system, macroH2A1 is not restricted to sites of DSBs, but comprises the entirety of the chromatin, suggesting that restricting its action locally is critical for promoting genome stability. Interestingly, certain clones of histone humanized yeasts with macroH2A1-HF-sb that lacked chromosomal rearrangements carried mutations in genes involved in HR-directed repair of DNA damage (*rad54*-S121R; Table S3), perhaps suppressing the effects of macroH2A1 HFD. Breakpoints of the chromosomal rearrangements in macroH2A1 humanized yeasts mapped to Ty elements, LTRs, sub-telomeres, and tRNAs (Table S5), suggesting that these repetitive regions become fragile when chromatinized with macroH2A1-HF-sb. Moreover, the chromatin decompaction in histone humanized yeast with either macroH2A1-HF-sb or H2Amacro1.2 may facilitate increased interactions between distantly located repetitive elements.

The humanized yeasts were generated in the mutant *DAD1*^{E50D} background, which we have previously shown to facilitate the purge of aneuploidies in histone humanized yeast.[31] Remarkably, all macroH2A1-HF-sb and H2Amacro1.2 humanized yeasts had at least one or more aneuploid chromosomes despite the *DAD1*^{E50D} mutation (Table S3), suggesting that both the histone fold and macro domain of macroH2A1 interfere with the adaptive benefit of the *DAD1*^{E50D} mutation. Potentially, increased aneuploidy could affect nucleosome positioning since gene dosage effects may lead to a gene spending more time in the non-expressed state. We do not think this is the case here. First, we have previously isolated massively aneuploid histone humanized yeasts (with the scc4^{D65Y} mutation). However, these strains showed no changes to nucleosome positions, demonstrating that aneuploidy alone is insufficient to trigger shifts in nucleosome positions.[5,31] Second, we show here that transcript abundance correlates one-to-one with aneuploidy level, suggesting no transcription dosage effects (Figure S11A). Third, we have previously shown that mRNA levels are reduced 6- to 8-fold in histone humanized yeast, yet no changes in nucleosome positioning were observed, indicating the time a gene spends in the "expressed" state does not influence nucleosome positions.[5] Instead, we conclude that changes to nucleosome positions are independent of aneuploid levels and that the increased rate of CIN is a result of macroH2A1.2 interfering with the centromeric chromatin, consistent with the negative GIs we observed between macroH2A1.2 overexpression and various kinetochore genes (Figure S2).

The *in vivo* manipulations of human variant histones in yeast set the stage for the reconstitution of more complex complements of histones. However, the ability to swap histone variants that define species-specific chromatin environments (e.g., point centromeres versus regional centromeres) may be an increasingly complex task, as highlighted by our recent attempts to directly replace the yeast centromeric histone, Cse4, with its human ortholog, CENP-A.[54] As such, future efforts in this system should aim to reconstitute chromatin not only at the nucleosome level but also include species-specific protein-protein interactions, such as chromatin remodelers, to determine factors that regulate chromatin structure and function *in vivo*.

Limitations of the study

Our histone shuffle system, while powerful for ease of manipulating the makeup of chromatin, has its set of drawbacks. First, as we encode histones on minimal centromeric plasmids, we cannot precisely control the copy number of histone genes across experiments. This is highlighted by the observations that macroH2A1.2 shows reduced expression compared to *Hs*H2A even though they are expressed from the same promoter (Figures 2A and 2B). Thus, copy-number alterations of the plasmids encoding histone genes may impact the variability or success of isolating histone humanized yeast. Second, our screen of nonessential gene deletions did not determine the relative levels of macroH2A1.2 overexpression compared to native histones. Nonetheless, previous overexpression experiments of histone H3 from a galactose-inducible promoter showed that the ectopically expressed histone represented half of all incorporated H3.[55] Third, we performed our experiments in the

background of the Dad1^{E50D} mutant. Thus, we cannot exclude the possibility that failure to isolate certain histone variant humanized yeasts may be contingent on this mutation. Lastly, our histone replacement method ensures that the entire histone pool is made up of the incoming set of histone genes. This is very different from what is natively found in human cells; for example, macroH2As make up only ~1% of the H2A histone pool.[56] While synthetic, our system of forcing yeast to subsist solely on a defined set of histones ultimately allows us to isolate their properties *in vivo*.

STAR★METHODS

Detailed methods are provided in the online version of this paper and include the following:

- KEY RESOURCES TABLE
- RESOURCE AVAILABILITY
  - Lead contact
  - Materials availability
  - Data and code availability
- EXPERIMENTAL MODEL AND SUBJECT DETAILS
  - Strains, plasmids, and oligos used
- METHOD DETAILS
  - Histone Humanization assay
  - Protein extraction and western blotting
  - Histone fluorescence protein tag and imaging
  - macroH2A1 overexpression and growth assay
  - High-throughput genetic interactions screen
  - Histone Humanized yeast plate reader growth assays
  - Construction of an expanded set of histones expressing plasmids
  - *SWR1* CRISPR/Cas9 deletions
  - Mapping the inviability of macroH2A1 histone fold
  - MNase digestions and sequencing
  - Capillary electrophoresis and NRL estimate
  - MNase sequencing data analysis
  - RNA extraction, sequencing, and nucleosome positioning analysis of differentially expressed genes
  - HiC libraries and analysis
  - Whole genome sequencing
  - Nanopore sequencing and analysis

SUPPLEMENTAL INFORMATION

Supplemental information can be found online at https://doi.org/10.1016/j.celrep.2024.114472.

ACKNOWLEDGMENTS

We are thankful to members of the Boeke lab for their helpful critiques and comments on the data presented here and to Dr. Chris Todd Hittinger and Dr. Emilyclare Baker for the *Saccharomyces eubayanus* strain yHEB1515, from which we sourced the histone promoters and genes. This work was supported by NIH (National Institute of General Medical Sciences [NIGMS]) fellowship F32GM116411 to D.M.T., a Genome Integrity Training Program NIH (NIGMS) T32GM115313 to M.A.B.H., and a Rules of Life: Epigenetics 2 grant from the NSF (National Science Foundation, award no. MCB-1921641) to J.D.B.

AUTHOR CONTRIBUTIONS

M.A.B.H., L.L.-S., D.M.T., and J.D.B. designed the research. M.A.B.H., L.L.-S., G.O., A.W., D.M.T., and M.J.S. carried out the experimental work. M.A.B.H., G.O., and L.L.-S. performed the data analysis. M.A.B.H. wrote the original manuscript draft and prepared the figures; M.A.B.H., L.L.-S, D.M.T., and J.D.B. edited the manuscript.

DECLARATION OF INTERESTS

J.D.B. is a founder and director of CDI Labs; a founder of and consultant to Opentrons Labworks/Neochromosome; and serves or served on the scientific advisory board of the following: CZ BioHub NY LLC, Logomix, Sangamo, Modern Meadow, Rome Therapeutics, SeaHub, Tessera Therapeutics, and the Wyss Institute.

Received: May 1, 2023
Revised: January 15, 2024
Accepted: June 24, 2024
Published: July 10, 2024

REFERENCES

1. Kornberg, R.D. (1974). Chromatin structure: a repeating unit of histones and DNA. Science *184*, 868–871. https://doi.org/10.1126/science.184.4139.868.
2. Luger, K., Mäder, A.W., Richmond, R.K., Sargent, D.F., and Richmond, T.J. (1997). Crystal structure of the nucleosome core particle at 2.8 A resolution. Nature *389*, 251–260. https://doi.org/10.1038/38444.
3. Marzluff, W.F., Wagner, E.J., and Duronio, R.J. (2008). Metabolism and regulation of canonical histone mRNAs: life without a poly(A) tail. Nat. Rev. Genet. *9*, 843–854. https://doi.org/10.1038/nrg2438.
4. Marzluff, W.F. (2005). Metazoan replication-dependent histone mRNAs: a distinct set of RNA polymerase II transcripts. Curr. Opin. Cell Biol. *17*, 274–280. https://doi.org/10.1016/j.ceb.2005.04.010.
5. Truong, D.M., and Boeke, J.D. (2017). Resetting the Yeast Epigenome with Human Nucleosomes. Cell *171*, 1508–1519.e13. https://doi.org/10.1016/j.cell.2017.10.043.
6. Talbert, P.B., and Henikoff, S. (2017). Histone variants on the move: substrates for chromatin dynamics. Nat. Rev. Mol. Cell Biol. *18*, 115–126. https://doi.org/10.1038/nrm.2016.148.
7. Talbert, P.B., and Henikoff, S. (2010). Histone variants — ancient wrap artists of the epigenome. Nat. Rev. Mol. Cell Biol. *11*, 264–275. https://doi.org/10.1038/nrm2861.
8. Martire, S., and Banaszynski, L.A. (2020). The roles of histone variants in fine-tuning chromatin organization and function. Nat. Rev. Mol. Cell Biol. *21*, 522–541. https://doi.org/10.1038/s41580-020-0262-8.
9. Malik, H.S., and Henikoff, S. (2003). Phylogenomics of the nucleosome. Nat. Struct. Biol. *10*, 882–891. https://doi.org/10.1038/nsb996.
10. Guberovic, I., Hurtado-Bagès, S., Rivera-Casas, C., Knobloch, G., Malinverni, R., Valero, V., Leger, M.M., García, J., Basquin, J., Gómez de Cedrón, M., et al. (2021). Evolution of a histone variant involved in compartmental regulation of NAD metabolism. Nat. Struct. Mol. Biol. *28*, 1009–1019. https://doi.org/10.1038/s41594-021-00692-5.
11. Guberovic, I., Farkas, M., Corujo, D., and Buschbeck, M. (2023). Evolution, structure and function of divergent macroH2A1 splice isoforms. Semin. Cell Dev. Biol. *135*, 43–49. https://doi.org/10.1016/j.semcdb.2022.03.036.
12. Molaro, A., Young, J.M., and Malik, H.S. (2018). Evolutionary origins and diversification of testis-specific short histone H2A variants in mammals. Genome Res. *28*, 460–473. https://doi.org/10.1101/gr.229799.117.
13. Zlatanova, J., and Thakar, A. (2008). H2A.Z: View from the Top. Structure *16*, 166–179. https://doi.org/10.1016/j.str.2007.12.008.
14. Santaguida, S., and Musacchio, A. (2009). The life and miracles of kinetochores. EMBO J. *28*, 2511–2531. https://doi.org/10.1038/emboj.2009.173.
15. Bryant, J.M., Govin, J., Zhang, L., Donahue, G., Pugh, B.F., and Berger, S.L. (2012). The Linker Histone Plays a Dual Role during Gametogenesis in Saccharomyces cerevisiae. Mol. Cell Biol. *32*, 2771–2783. https://doi.org/10.1128/MCB.00282-12.

16. Pehrson, J.R., and Fried, V.A. (1992). MacroH2A, a Core Histone Containing a Large Nonhistone Region. Science *257*, 1398–1400. https://doi.org/10.1126/science.1529340.

17. Chakravarthy, S., and Luger, K. (2006). The Histone Variant Macro-H2A Preferentially Forms "Hybrid Nucleosomes.". J. Biol. Chem. *281*, 25522–25531. https://doi.org/10.1074/jbc.M602258200.

18. Chang, E.Y., Ferreira, H., Somers, J., Nusinow, D.A., Owen-Hughes, T., and Narlikar, G.J. (2008). MacroH2A Allows ATP-Dependent Chromatin Remodeling by SWI/SNF and ACF Complexes but Specifically Reduces Recruitment of SWI/SNF. Biochemistry *47*, 13726–13732. https://doi.org/10.1021/bi8016944.

19. Angelov, D., Molla, A., Perche, P.-Y., Hans, F., Côté, J., Khochbin, S., Bouvet, P., and Dimitrov, S. (2003). The Histone Variant MacroH2A Interferes with Transcription Factor Binding and SWI/SNF Nucleosome Remodeling. Mol. Cell *11*, 1033–1041. https://doi.org/10.1016/S1097-2765(03)00100-X.

20. Gamble, M.J., Frizzell, K.M., Yang, C., Krishnakumar, R., and Kraus, W.L. (2010). The histone variant macroH2A1 marks repressed autosomal chromatin, but protects a subset of its target genes from silencing. Genes Dev. *24*, 21–32. https://doi.org/10.1101/gad.1876110.

21. Jiang, C., and Pugh, B.F. (2009). A compiled and systematic reference map of nucleosome positions across the Saccharomyces cerevisiae genome. Genome Biol. *10*, R109. https://doi.org/10.1186/gb-2009-10-10-r109.

22. Lai, W.K.M., and Pugh, B.F. (2017). Understanding nucleosome dynamics and their links to gene expression and DNA replication. Nat. Rev. Mol. Cell Biol. *18*, 548–562. https://doi.org/10.1038/nrm.2017.47.

23. Hartley, P.D., and Madhani, H.D. (2009). Mechanisms that specify promoter nucleosome location and identity. Cell *137*, 445–458. https://doi.org/10.1016/j.cell.2009.02.043.

24. Krietenstein, N., Wal, M., Watanabe, S., Park, B., Peterson, C.L., Pugh, B.F., and Korber, P. (2016). Genomic Nucleosome Organization Reconstituted with Pure Proteins. Cell *167*, 709–721.e12. https://doi.org/10.1016/j.cell.2016.09.045.

25. Oberbeckmann, E., Krietenstein, N., Niebauer, V., Wang, Y., Schall, K., Moldt, M., Straub, T., Rohs, R., Hopfner, K.-P., Korber, P., and Eustermann, S. (2021). Genome information processing by the INO80 chromatin remodeler positions nucleosomes. Nat. Commun. *12*, 3231. https://doi.org/10.1038/s41467-021-23016-z.

26. Oberbeckmann, E., Niebauer, V., Watanabe, S., Farnung, L., Moldt, M., Schmid, A., Cramer, P., Peterson, C.L., Eustermann, S., Hopfner, K.-P., and Korber, P. (2021). Ruler elements in chromatin remodelers set nucleosome array spacing and phasing. Nat. Commun. *12*, 3232. https://doi.org/10.1038/s41467-021-23015-0.

27. Zhang, Z., Wippo, C.J., Wal, M., Ward, E., Korber, P., and Pugh, B.F. (2011). A packing mechanism for nucleosome organization reconstituted across a eukaryotic genome. Science *332*, 977–980. https://doi.org/10.1126/science.1200508.

28. Gossett, A.J., and Lieb, J.D. (2012). In vivo effects of histone H3 depletion on nucleosome occupancy and position in Saccharomyces cerevisiae. PLoS Genet. *8*, e1002771. https://doi.org/10.1371/journal.pgen.1002771.

29. Lieleg, C., Ketterer, P., Nuebler, J., Ludwigsen, J., Gerland, U., Dietz, H., Mueller-Planitz, F., and Korber, P. (2015). Nucleosome spacing generated by ISWI and CHD1 remodelers is constant regardless of nucleosome density. Mol. Cell Biol. *35*, 1588–1605. https://doi.org/10.1128/MCB.01070-14.

30. Haase, M.A.B., Truong, D.M., and Boeke, J.D. (2019). Superloser: A Plasmid Shuffling Vector for Saccharomyces cerevisiae with Exceedingly Low Background. G3 (Bethesda). *9*, 2699–2707. https://doi.org/10.1534/g3.119.400325.

31. Haase, M.A.B., Ólafsson, G., Flores, R.L., Boakye-Ansah, E., Zelter, A., Dickinson, M.S., Lazar-Stefanita, L., Truong, D.M., Asbury, C.L., Davis, T.N., and Boeke, J.D. (2023). DASH/Dam1 complex mutants stabilize ploidy in histone-humanized yeast by weakening kinetochore-microtubule attachments. EMBO J. *42*, e112600. https://doi.org/10.15252/embj.2022112600.

32. Haase, M.A.B., Steenwyk, J.L., and Boeke, J.D. (2023). Gene loss and cis-regulatory novelty shaped core histone gene evolution in the apiculate yeast *Hanseniaspora uvarum*. bioRxiv. https://doi.org/10.1101/2023.08.28.551515.

33. McBurney, K.L., Leung, A., Choi, J.K., Martin, B.J.E., Irwin, N.A.T., Bartke, T., Nelson, C.J., and Howe, L.J. (2016). Divergent Residues Within Histone H3 Dictate a Unique Chromatin Structure in *Saccharomyces cerevisiae*. Genetics *202*, 341–349. https://doi.org/10.1534/genetics.115.180810.

34. Urahama, T., Harada, A., Maehara, K., Horikoshi, N., Sato, K., Sato, Y., Shiraishi, K., Sugino, N., Osakabe, A., Tachiwana, H., et al. (2016). Histone H3.5 forms an unstable nucleosome and accumulates around transcription start sites in human testis. Epigenet. Chromatin *9*, 2. https://doi.org/10.1186/s13072-016-0051-y.

35. Zalensky, A.O., Siino, J.S., Gineitis, A.A., Zalenskaya, I.A., Tomilin, N.V., Yau, P., and Bradbury, E.M. (2002). Human testis/sperm-specific histone H2B (hTSH2B). Molecular cloning and characterization. J. Biol. Chem. *277*, 43474–43480. https://doi.org/10.1074/jbc.M206065200.

36. Tachiwana, H., Kagawa, W., Osakabe, A., Kawaguchi, K., Shiga, T., Hayashi-Takanaka, Y., Kimura, H., and Kurumizaka, H. (2010). Structural basis of instability of the nucleosome containing a testis-specific histone variant, human H3T. Proc. Natl. Acad. Sci. USA *107*, 10454–10459. https://doi.org/10.1073/pnas.1003064107.

37. Wood, T.J., Thistlethwaite, A., Harris, M.R., Lovell, S.C., and Millar, C.B. (2013). Mutations in Non-Acid Patch Residues Disrupt H2A.Z's Association with Chromatin through Multiple Mechanisms. PLoS One *8*, e76394. https://doi.org/10.1371/journal.pone.0076394.

38. Clarkson, M.J., Wells, J.R., Gibson, F., Saint, R., and Tremethick, D.J. (1999). Regions of variant histone His2AvD required for Drosophila development. Nature *399*, 694–697. https://doi.org/10.1038/21436.

39. Bowerman, S., Hickok, R.J., and Wereszczynski, J. (2019). Unique Dynamics in Asymmetric macroH2A–H2A Hybrid Nucleosomes Result in Increased Complex Stability. J. Phys. Chem. B *123*, 419–427. https://doi.org/10.1021/acs.jpcb.8b10668.

40. Iwasaki, W., Miya, Y., Horikoshi, N., Osakabe, A., Taguchi, H., Tachiwana, H., Shibata, T., Kagawa, W., and Kurumizaka, H. (2013). Contribution of histone N-terminal tails to the structure and stability of nucleosomes. FEBS Open Bio *3*, 363–369. https://doi.org/10.1016/j.fob.2013.08.007.

41. Lee, K.P., Baxter, H.J., Guillemette, J.G., Lawford, H.G., and Lewis, P.N. (1982). Structural studies on yeast nucleosomes. Can. J. Biochem. *60*, 379–388. https://doi.org/10.1139/o82-045.

42. Piñeiro, M., Puerta, C., and Palacián, E. (1991). Yeast nucleosomal particles: structural and transcriptional properties. Biochemistry *30*, 5805–5810. https://doi.org/10.1021/bi00237a025.

43. Leung, A., Cheema, M., González-Romero, R., Eirin-Lopez, J.M., Ausió, J., and Nelson, C.J. (2016). Unique yeast histone sequences influence octamer and nucleosome stability. FEBS Lett. *590*, 2629–2638. https://doi.org/10.1002/1873-3468.12266.

44. Lazar-Stefanita, L., Haase, M.A.B., and Boeke, J.D. (2023). Humanized nucleosomes reshape replication initiation and rDNA/nucleolar integrity in yeast. bioRxiv. https://doi.org/10.1101/2023.05.06.539710.

45. Park, D., Morris, A.R., Battenhouse, A., and Iyer, V.R. (2014). Simultaneous mapping of transcript ends at single-nucleotide resolution and identification of widespread promoter-associated non-coding RNA governed by TATA elements. Nucleic Acids Res. *42*, 3736–3749. https://doi.org/10.1093/nar/gkt1366.

46. Grigoryev, S.A. (2012). Nucleosome spacing and chromatin higher-order folding. Nucleus *3*, 493–499. https://doi.org/10.4161/nucl.22168.

47. Correll, S.J., Schubert, M.H., and Grigoryev, S.A. (2012). Short nucleosome repeats impose rotational modulations on chromatin fibre folding. EMBO J. *31*, 2416–2426. https://doi.org/10.1038/emboj.2012.80.

48. Ni, K., and Muegge, K. (2021). LSH catalyzes ATP-driven exchange of histone variants macroH2A1 and macroH2A2. Nucleic Acids Res. *49*, 8024–8036. https://doi.org/10.1093/nar/gkab588.

49. Litwin, I., Bakowski, T., Szakal, B., Pilarczyk, E., Maciaszczyk-Dziubinska, E., Branzei, D., and Wysocki, R. (2018). Error-free DNA damage tolerance pathway is facilitated by the Irc5 translocase through cohesin. EMBO J. *37*, e98732. https://doi.org/10.15252/embj.201798732.

50. Singh, A.K., Schauer, T., Pfaller, L., Straub, T., and Mueller-Planitz, F. (2021). The biogenesis and function of nucleosome arrays. Nat. Commun. *12*, 7011. https://doi.org/10.1038/s41467-021-27285-6.

51. Sebastian, R., Hosogane, E.K., Sun, E.G., Tran, A.D., Reinhold, W.C., Burkett, S., Sturgill, D.M., Gudla, P.R., Pommier, Y., Aladjem, M.I., and Oberdoerffer, P. (2020). Epigenetic Regulation of DNA Repair Pathway Choice by MacroH2A1 Splice Variants Ensures Genome Stability. Mol. Cell *79*, 836–845.e7. https://doi.org/10.1016/j.molcel.2020.06.028.

52. Khurana, S., Kruhlak, M.J., Kim, J., Tran, A.D., Liu, J., Nyswaner, K., Shi, L., Jailwala, P., Sung, M.-H., Hakim, O., and Oberdoerffer, P. (2014). A macrohistone variant links dynamic chromatin compaction to BRCA1-dependent genome maintenance. Cell Rep. *8*, 1049–1062. https://doi.org/10.1016/j.celrep.2014.07.024.

53. Kim, J., Sturgill, D., Sebastian, R., Khurana, S., Tran, A.D., Edwards, G.B., Kruswick, A., Burkett, S., Hosogane, E.K., Hannon, W.W., et al. (2018). Replication Stress Shapes a Protective Chromatin Environment across Fragile Genomic Regions. Mol. Cell *69*, 36–47.e7. https://doi.org/10.1016/j.molcel.2017.11.021.

54. Ólafsson, G., Haase, M.A.B., and Boeke, J.D. (2023). Humanization reveals pervasive incompatibility of yeast and human kinetochore components. G3 (Bethesda). *14*, jkad260. https://doi.org/10.1093/g3journal/jkad260.

55. Jamai, A., Imoberdorf, R.M., and Strubin, M. (2007). Continuous Histone H2B and Transcription-Dependent Histone H3 Exchange in Yeast Cells outside of Replication. Mol. Cell *25*, 345–355. https://doi.org/10.1016/j.molcel.2007.01.019.

56. Buschbeck, M., and Hake, S.B. (2017). Variants of core histones and their roles in cell fate decisions, development and cancer. Nat. Rev. Mol. Cell Biol. *18*, 299–314. https://doi.org/10.1038/nrm.2016.166.

57. Brachmann, C.B., Davies, A., Cost, G.J., Caputo, E., Li, J., Hieter, P., and Boeke, J.D. (1998). Designer deletion strains derived from Saccharomyces cerevisiae S288C: A useful set of strains and plasmids for PCR-mediated gene disruption and other applications. Yeast *14*, 115–132.

58. Schindelin, J., Arganda-Carreras, I., Frise, E., Kaynig, V., Longair, M., Pietzsch, T., Preibisch, S., Rueden, C., Saalfeld, S., Schmid, B., et al. (2012). Fiji: an open-source platform for biological-image analysis. Nat. Methods *9*, 676–682. https://doi.org/10.1038/nmeth.2019.

59. Li, H., Handsaker, B., Wysoker, A., Fennell, T., Ruan, J., Homer, N., Marth, G., Abecasis, G., and Durbin, R.; 1000 Genome Project Data Processing Subgroup (2009). The Sequence Alignment/Map format and SAMtools. Bioinformatics *25*, 2078–2079. https://doi.org/10.1093/bioinformatics/btp352.

60. Langmead, B., and Salzberg, S.L. (2012). Fast gapped-read alignment with Bowtie 2. Nat. Methods *9*, 357–359. https://doi.org/10.1038/nmeth.1923.

61. Bolger, A.M., Lohse, M., and Usadel, B. (2014). Trimmomatic: a flexible trimmer for Illumina sequence data. Bioinformatics *30*, 2114–2120. https://doi.org/10.1093/bioinformatics/btu170.

62. Li, H., and Durbin, R. (2009). Fast and accurate short read alignment with Burrows-Wheeler transform. Bioinformatics *25*, 1754–1760. https://doi.org/10.1093/bioinformatics/btp324.

63. Chen, K., Xi, Y., Pan, X., Li, Z., Kaestner, K., Tyler, J., Dent, S., He, X., and Li, W. (2013). DANPOS: Dynamic analysis of nucleosome position and occupancy by sequencing. Genome Res. *23*, 341–351. https://doi.org/10.1101/gr.142067.112.

64. Serizay, J., and Ahringer, J. (2021). Generating fragment density plots in R/Bioconductor with VplotR. JOSS *6*, 3009. https://doi.org/10.21105/joss.03009.

65. Chen, C., Chen, H., Zhang, Y., Thomas, H.R., Frank, M.H., He, Y., and Xia, R. (2020). TBtools: An Integrative Toolkit Developed for Interactive Analyses of Big Biological Data. Mol. Plant *13*, 1194–1202. https://doi.org/10.1016/j.molp.2020.06.009.

66. Belyeu, J.R., Chowdhury, M., Brown, J., Pedersen, B.S., Cormier, M.J., Quinlan, A.R., and Layer, R.M. (2021). Samplot: a platform for structural variant visual validation and automated filtering. Genome Biol. *22*, 161. https://doi.org/10.1186/s13059-021-02380-5.

67. Li, H. (2018). Minimap2: pairwise alignment for nucleotide sequences. Bioinformatics *34*, 3094–3100. https://doi.org/10.1093/bioinformatics/bty191.

68. Smolka, M., Paulin, L.F., Grochowski, C.M., Horner, D.W., Mahmoud, M., Behera, S., Kalef-Ezra, E., Gandhi, M., Hong, K., Pehlivan, D., et al. (2022). Comprehensive Structural Variant Detection: From Mosaic to Population-Level. bioRxiv. https://doi.org/10.1101/2022.04.04.487055.

69. Jiang, T., Liu, Y., Jiang, Y., Li, J., Gao, Y., Cui, Z., Liu, Y., Liu, B., and Wang, Y. (2020). Long-read-based human genomic structural variation detection with cuteSV. Genome Biol. *21*, 189. https://doi.org/10.1186/s13059-020-02107-y.

70. Rausch, T., Hsi-Yang Fritz, M., Korbel, J.O., and Benes, V. (2019). Alfred: interactive multi-sample BAM alignment statistics, feature counting and feature annotation for long- and short-read sequencing. Bioinformatics *35*, 2489–2491. https://doi.org/10.1093/bioinformatics/bty1007.

71. Ólafsson, G., and Thorpe, P.H. (2020). Polo kinase recruitment via the constitutive centromere-associated network at the kinetochore elevates centromeric RNA. PLoS Genet. *16*, e1008990. https://doi.org/10.1371/journal.pgen.1008990.

72. Reid, R.J.D., Du, X., Sunjevaric, I., Rayannavar, V., Dittmar, J., Bryant, E., Maurer, M., and Rothstein, R. (2016). A Synthetic Dosage Lethal Genetic Interaction Between *CKS1B* and *PLK1* Is Conserved in Yeast and Human Cancer Cells. Genetics *204*, 807–819. https://doi.org/10.1534/genetics.116.190231.

73. León Ortiz, A.M., Reid, R.J.D., Dittmar, J.C., Rothstein, R., and Nicolas, A. (2011). Srs2 overexpression reveals a helicase-independent role at replication forks that requires diverse cell functions. DNA Repair *10*, 506–517. https://doi.org/10.1016/j.dnarep.2011.02.004.

74. Reid, R.J.D., González-Barrera, S., Sunjevaric, I., Alvaro, D., Ciccone, S., Wagner, M., and Rothstein, R. (2011). Selective ploidy ablation, a high-throughput plasmid transfer protocol, identifies new genes affecting topoisomerase I–induced DNA damage. Genome Res. *21*, 477–486. https://doi.org/10.1101/gr.109033.110.

75. Winzeler, E.A., Shoemaker, D.D., Astromoff, A., Liang, H., Anderson, K., Andre, B., Bangham, R., Benito, R., Boeke, J.D., Bussey, H., et al. (1999). Functional Characterization of the *S. cerevisiae* Genome by Gene Deletion and Parallel Analysis. Science *285*, 901–906. https://doi.org/10.1126/science.285.5429.901.

76. Dittmar, J.C., Reid, R.J., and Rothstein, R. (2010). ScreenMill: A freely available software suite for growth measurement, analysis and visualization of high-throughput screen data. BMC Bioinf. *11*, 353. https://doi.org/10.1186/1471-2105-11-353.

77. Klemm, C., Howell, R.S.M., and Thorpe, P.H. (2022). ScreenGarden: a shinyR application for fast and easy analysis of plate-based high-throughput screens. BMC Bioinf. *23*, 60. https://doi.org/10.1186/s12859-022-04586-1.

78. Chakravarthy, S., Gundimella, S.K.Y., Caron, C., Perche, P.-Y., Pehrson, J.R., Khochbin, S., and Luger, K. (2005). Structural characterization of the histone variant macroH2A. Mol. Cell Biol. *25*, 7616–7624. https://doi.org/10.1128/MCB.25.17.7616-7624.2005.

79. Serizay, J., Dong, Y., Jänes, J., Chesney, M., Cerrato, C., and Ahringer, J. (2020). Distinctive regulatory architectures of germline-active and somatic genes in *C. elegans*. Genome Res. *30*, 1752–1765. https://doi.org/10.1101/gr.265934.120.

80. Ge, S.X., Jung, D., and Yao, R. (2020). ShinyGO: a graphical gene-set enrichment tool for animals and plants. Bioinformatics *36*, 2628–2629. https://doi.org/10.1093/bioinformatics/btz931.

81. Lazar-Stefanita, L., Luo, J., Montagne, R., Thierry, A., Sun, X., Mercy, G., Mozziconacci, J., Koszul, R., and Boeke, J.D. (2022). Karyotype engineering reveals spatio-temporal control of replication firing and gene contacts. Cell Genom. *2*, 100163. https://doi.org/10.1016/j.xgen.2022.100163.

82. Lazar-Stefanita, L., Scolari, V.F., Mercy, G., Muller, H., Guérin, T.M., Thierry, A., Mozziconacci, J., and Koszul, R. (2017). Cohesins and condensins orchestrate the 4D dynamics of yeast chromosomes during the cell cycle. EMBO J. *36*, 2684–2697. https://doi.org/10.15252/embj.201797342.

STAR★METHODS

KEY RESOURCES TABLE

REAGENT or RESOURCE	SOURCE	IDENTIFIER
Antibodies		
Rabbit anti-GFP	Torrey Pines Scientific	Cat#TP401
Mouse anti-alpha-tubulin	SIGMA	Cat#T5168
IRDye® 800CW Goat anti-Mouse IgG	LiCoR	Cat#926-32210
IRDye® 680RD Goat anti-Rabbit IgG	LI-COR	Cat#926-68071
Chemicals, peptides, and recombinant proteins		
5-Fluoroorotic Acid Monohydrate (FOA, 5-FOA)	US Biological	Cat#F5050
TWEEN® 20	Sigma-Aldrich	Cat#P1379
cOmplete™, EDTA-free Protease Inhibitor Cocktail	Sigma-Aldrich	Cat#11873580001
Lysing Matrix Y, 2 mL tube	MP Biomedicals	Cat#116960100
NuPAGE™ 12% Bis-Tris Protein Gels, 1.0 mm, 12-well	Thermo Fisher Scientific	Cat#NP0342BOX
NuPAGE™ MES SDS Running Buffer (20X)	Thermo Fisher Scientific	Cat#NP000202
Trans-Blot	Bio-Rad	Cat#1704275
Blocking buffer Intercept	LiCoR	Cat#927-70001
Concanavalin a from Canavalia ensiformis (Jack bean),Type VI, lyophilized powder	Sigma-Aldrich	Cat#L7647-250MG
BssHII	New England Biolabs (NEB)	Cat#R0199L
Micrococcal Nuclease (300 U/μL)	Thermo Fisher Scientific	Cat#EN0181
Formaldehyde solution (Formalin)	Sigma-Aldrich	Cat#F8775-4X25ML
2-Mercaptoethanol, ≥99.0%	Sigma-Aldrich	Cat#M6250-10ML
Zymolyase 100T	USBiological	Cat#Z1004
DNaseI	Agilent	Cat#600031
RNAse A, DNase and protease-free	Thermo Fischer	Cat#EN0531
Proteinase K	Thermo Scientific	Cat#EO0492
UltraPure Dithiothreitol	Thermo Scientific	Cat#15508013
Phenol:Chloroform:Isoamyl alcohol	Thermo Scientific	Cat#15593
chloroform:isoamyl alcohol	Sigma-Aldrich	Cat#C0549-1QT
SERA-MAG beads	Cytiva	Cat#29343052
Critical commercial assays		
Zymo-Spin I Columns kit	Zymo Research	Cat#C1003-50
ZAG 135 dsDNA Kit (1-1500bp)	Agilent Technologies	Cat#ZAG-135-5000
QIAseq Stranded Total RNA Lib Kit	Qiagen	Cat#180745
QIAseq FastSelect–rRNA Yeast Kit	Qiagen	Cat#334217
NEBNext Ultra II FS kit	New England Biolabs (NEB)	Cat#E7805L
NEBNext Ultra II kit	New England Biolabs (NEB)	Cat#E7645L
Nextseq 500/550 High Output Kit v2.5 (150 Cycles)	Illumina	Cat# 20024907
NextSeq High-output 75-cycle V2.5 Kit	Illumina	Cat#20024906
Qubit™ 1X dsDNA HS Assay Kit	Thermo Scientific	Cat#Q33231
Oxford Nanopore Rapid Barcoding kit	Oxford Nanopore	Cat#SQK-RBK004
Minion R9.4.1 flow cell	Oxford Nanopore	Cat#FLO-MIN106.001
Deposited data		
Raw FASTQ files	This study	PRJNA950985
Experimental models: organisms/strains		
S. cerevisiae. Genotype: *MAT***a** *his3Δ1 leu2Δ0 met15Δ0 ura3Δ0*	Brachmann et al.[57]	BY4741

(*Continued on next page*)

Continued

REAGENT or RESOURCE	SOURCE	IDENTIFIER
S. cerevisiae. Genotype: *MAT***alpha** *his3Δ1 leu2Δ0 lys2Δ0 ura3Δ0*	Brachmann et al.[57]	BY4742
S. cerevisiae. Genotype: *MAT***a** *his1*	This study	yMAH652
S. cerevisiae. Genotype: *MAT***alpha** *his1*	This study	yMAH653
S. cerevisiae. Genotype: *MAT***alpha** *his3Δ200 leu2Δ0 lys2Δ0 trp1Δ63 ura3Δ0 met15Δ0 hta2-htb2Δ0 hta1-htb1Δ0 hht1-hhf1Δ0 hht2-hhf2Δ0 DAD1-E50D* [pDT139]	Haase et al.[31,32]	yMAH700
S. cerevisiae. Genotype: *MAT***alpha** *his3Δ200 leu2Δ0 lys2Δ0 trp1Δ63 ura3Δ0 met15Δ0 hta2-htb2Δ0 hta1-htb1Δ0 hht1-hhf1Δ0 hht2-hhf2Δ0* [pDT109]	Truong and Boeke[5]	yDT180
Software and algorithms		
GraphPad Prism version 9	GraphPad Software, San Diego, California USA,	http://www.graphpad.com/
ImageJ	Schindelin et al.[58]	https://imagej.nih.gov/ij/
MATLAB	MATLAB 2022a	https://www.mathworks.com/products/matlab.html
SAMtools version 1.9	Li et al.[59]	http://samtools.sourceforge.net/
Bowtie 2	Langmead and Salzberg[60]	http://bowtie-bio.sourceforge.net/bowtie2/index.shtml
Trimmomatic version 0.39	Bolger et al.[61]	http://www.usadellab.org/cms/?page=trimmomatic
FastQC version 0.11.4		https://github.com/s-andrews/FastQC
BWA version 0.7.7	Li and Durbin[62]	https://bio-bwa.sourceforge.net/
DANPOS version 2	Chen et al.[63]	https://sites.google.com/site/danposdoc/
R version 4.1.0		https://www.r-project.org/
VplotR version 1.2.0	Serizay and Ahringer[64]	https://github.com/js2264/VplotR
TBtools version 1.113	Chen et al.[65]	https://github.com/CJ-Chen/TBtools
Samplot version 1.3.0	Belyeu et al.[66]	https://github.com/ryanlayer/samplot
Minimap2 version 2.24	Li[67]	https://github.com/lh3/minimap2
Sniffles version 2.0.7	Smolka et al.[68]	https://github.com/fritzsedlazeck/Sniffles
CuteSV	Jiang et al.[69]	https://github.com/tjiangHIT/cuteSV
Porechop version 0.2.4		https://github.com/rrwick/Porechop
Alfred version 0.2.6	Rausch et al.[70]	https://github.com/tobiasrausch/alfred

RESOURCE AVAILABILITY

Lead contact

Further information and requests for resources and reagents should be directed to and will be fulfilled by the lead contact, Jef D. Boeke (jef.boeke@nyulangone.org).

Materials availability

All yeast strains and plasmids generated in this study are available from the lead contact upon request.

Data and code availability

- All sequencing data generated in this study (whole genome sequencing, HiC, RNA sequencing, and MNase sequencing) have been deposited to the sequence read archive (SRA) under the BioProject PRJNA950985. HiC data is accessible under the accessions SRA: SRX19844760 – SRX19844772. WGS, RNA-seq, and MNase-seq data is accessible under the accessions SRA: SRX19839443 – SRX19839498.
- This paper does not report original code.
- Additional supplemental data have been uploaded to FigShare under the https://doi.org/10.6084/m9.figshare.24941760.

EXPERIMENTAL MODEL AND SUBJECT DETAILS

Strains, plasmids, and oligos used

All strains and plasmids used in this study are listed in Table S1 and are available upon request. Strains were grown under standard laboratory conditions, either in rich medium (YPD) or synthetic complete (SC) dropout medium. Sequences of oligonucleotides used are provided in Table S1.

METHOD DETAILS

Histone Humanization assay

Unless otherwise indicated, histone Humanizations were performed in the *DAD1*^{E50D} dual-histone plasmid shuffle strain (yMAH700). The *DAD1*^{E50D} mutation improves humanization rates by a factor of ~10^4 by weakening kinetochore-microtubule interactions.[31] The shuffle strain, where a single set of yeast core histone genes is maintained on a counter-selectable plasmid (*URA3*; Superloser plasmid, pDT139), is transformed with the appropriate human histone plasmid (containing the *TRP1* marker). This "Superloser" plasmid can be destabilized following the addition of galactose, using a *GAL10* promoter adjacent to the *CEN* sequence, and then swapped for an orthogonal plasmid containing a full complement of human histones by using the 5-FOA negative selection.[30] This forces yeast to subsist solely on the incoming human histone plasmid. Once transformants were visible, three clones were inoculated into 5 mL of SC–TRP+GAL/RAF liquid medium and grown until saturation (typically 2 days). Culture absorbance (A_{600}) was measured, and then 1μL, 10μL, 100μL, and 1mL of the saturated culture was plated to SC–TRP+5FOA agar plates. Agar plates were then incubated at 30°C for up to three months within a sealed container with damp paper towels to maintain moisture. Only colonies appearing after 2 weeks of incubation were counted, and PCR genotyped to verify the loss of yeast histones as previously described.[30,31] Humanization frequencies were then determined by dividing the colony-forming units by the total number of cells plated. The empty vector swap determines the assay background, in which plasmid recombinants or spontaneous *ura3* mutants bypass 5-FOA selection at an average rate of ~1 in 10 million cells. In some cases, where indicated, the humanization frequencies were normalized to the value of humanization for replicative human histones.

Protein extraction and western blotting

Immunoblotting of macroH2A-GFP (plasmid pMAH276) and human H2A-GFP (plasmid pMAH282) was performed in the wild-type shuffle strain (yDT67). Briefly, strains were first transformed with a *URA3* plasmid encoding four human histones (with either macroH2A-GFP or human H2A-GFP, in addition to human H3.1, H4, and H2B). Transformants were then grown at 30°C overnight in SC–Ura medium and the following morning diluted in fresh medium and grown until mid-log phase (A_{600} ~ 0.8–1.0). Cultures were then collected with centrifugation, washed once with water, and resuspended in lysis buffer (40mM HEPES-NaOH, pH 7.5, 350 mM NaCl, 0.1% Tween 20, 10% glycerol) + protease inhibitors (cOmplete)). Resuspensions were transferred to tubes with a pre-aliquoted amount of 0.5 mm diameter yttria-stabilized zirconium oxide beads, and cells were disrupted at 4°C using the MP-Bio FastPrep-24 lysis system. Lysate was centrifuged at maximum speed for 25 min and clarified lysate was used for western blotting.

Approximately 10 μg of protein was loaded on a 12% Bis-Tris NuPAGE gel in MES buffer. Protein was then transferred to 45 μm LF PVDF membranes using the Bio-Rad Trans-Blot Turbo system, following the manufacturer's specification and using the mixed molecular weight preset. Transferred membranes were then blocked for 1 h at room temperature with a 1:1 solution of TBS buffer and LiCor blocking buffer. Next, membranes were incubated overnight at 4°C with primary antibodies in a 1:1 solution of TBST (TBS +0.05% Tween 20) and LiCor blocking buffer (Rabbit anti-GFP, Torrey Pines Scientific TP401; and Mouse anti-alpha-tubulin, Sigma T5168). Membranes were then washed 5x times with TBST, with incubations of 10 min between washes at room temperature. Then membranes were incubated with fluorescent secondary antibodies (IRDye 800CW Goat anti-Mouse IgG and IRDye 680RD Goat anti-Rabbit IgG) in a 1:1 solution of TBST and LiCor blocking buffer with 0.01% SDS for 1.5 h at room temperature. Finally, membranes were washed 5x times with TBST, with incubations of 10 min between washes at room temperature, and imaged using an Odyssey imaging system.

Histone fluorescence protein tag and imaging

Fluorescence imaging of macroH2A-GFP and human H2A-GFP was performed in the wild-type shuffle strain with a nuclear envelope RFP tag (Nup49-RFP; strain yMAH1279). Briefly, strains were first transformed with a *URA3* plasmid encoding four human histones (with either macroH2A-GFP or human H2A-GFP, in addition to human H3.1, H4, and H2B). Transformants were then grown at 30°C overnight in SC–Ura medium and the following morning diluted in fresh medium and grown until mid-log phase (A_{600} ~ 0.6–0.8). Cells were then adhered to the surface of an ibidi μ-slide VI with Concanavalin A from *Canavalia ensiformis* (10 mg/mL in water) and imaged using an EVOS M7000. Scale bars were added to micrographs and cropped using the ImageJ software.[58]

macroH2A1 overexpression and growth assay

macroH2A1 was cloned into a galactose inducible CEN/ARS plasmid (pMAH692) and transformed into BY4741. Transformants were grown at 30°C overnight in SC–Leu and normalized to A_{600} ~1.0 the following morning and dotted out onto either SC–Leu or SC–Leu+Gal agar plates. Plates were incubated at 30°C for two days and then imaged.

High-throughput genetic interactions screen

The genetic interactions screen was performed as previously described.[71,72] We used a conditional overexpression plasmid containing a *LEU2* selectable marker and macroH2A1 driven by the *GAL1* promoter (pMAH692). Using a high-throughput, mating-based method, selective ploidy ablation (SPA),[73,74] we transferred the plasmid and an empty control plasmid into an array of the yeast deletion collection of non-essential genes, about 4800 strains in total.[75] The assay was performed using a semi-automatic robotic pinning system, the ROTOR HDA (Singer Instruments, UK), and rectangular agar plates containing the deletion collection previously arrayed as 384 different strains in quadruplicate per plate, i.e., at 1536 colony density. Each incubation step was performed at 30°C. The final SC–Leu 2% galactose 5-FOA agar plates of the assay were incubated for 4 days and imaged using a Scan Maker 9800XL Plus (Mikrotek) plate scanner. The colonies were analyzed using colony quantification software.[76,77] Colonies that grew poorly with the empty control plasmid were excluded from the analysis.

Histone Humanized yeast plate reader growth assays

The histone Humanized yeast, yDT180 (derived from the *DAD1*^{E50D} shuffle strain), was transformed with *URA3* CEN/ARS plasmids encoding a full complement of human histones (either all replicative histones (pMAH22) or a single variant with 3 replicative histones (e.g., human macroH2A1, *Hs*H2B, *Hs*H3.1, and *Hs*H4; pMAH87)) or encoding just *Hs*H2B, *Hs*H3.1, and *Hs*H4 (pMAH27). Transformations of histone Humanized yeast were modified as follows. A single colony to be transformed was grown until reaching saturation in YPD. The night before transforming, this culture was diluted 3:200 in fresh YPD and grown at 30°C for at least 12 h or until A_{600} ~0.6 was reached. From here, standard lithium acetate transformation procedures were followed. To ensure the isolation of transformants, we transformed at least 1 μg of plasmid DNA. Plates were left to incubate at 30°C for up to two weeks until transformants appeared.

Transformants were then cultured for 5 days in 5 mL of the appropriate liquid medium to maintain selection for both plasmids (SC–Trp–Ura). Once cultures reached saturation, they were diluted to A_{600} ~1.0, and this suspension was used to inoculate 220 μL of growth medium to a starting A_{600} of 0.1 in a 96-well flat-bottomed UV transparent plate. Growth was then monitored at 30°C for 120 h, with measurements of the A_{600} every 15 min, using EON Microplate Spectrophotometer (Biotek). Growth curves were analyzed using the manufacturer's supplied software and plotted in Prism.

Construction of an expanded set of histones expressing plasmids

To approach the experiment in Figures 2G and 2H, we needed an expanded set of orthologous histone promoters available for expressing core histones in *S. cerevisiae* (minimally, we needed six total promoters). This reduces sequence similarity between the two plasmids, thereby limiting plasmid recombination events.[30] To this end, we cloned the histone genes and promoters of the closely related species *S. eubayanus* into a counter-selectable *URA3* plasmid (Figures S4A and S4B). To ensure the histone loci of *S. eubayanus* function in *S. cerevisiae* we first PCR amplified and cloned each pair (SeHTA1B1HHF2T2; pMAH303 and *SeHTA2B2HHF1T1*; pMAH296) into a BssHII linearized *TRP1* CEN/ARS plasmid (pRS414) by yeast gap repair (Figures S4A and S4B). Plasmids were recovered from yeast, transformed in to bacteria, and verified by digestion. The viability of *S. eubayanus* histone genes and promoters were tested using our dual-plasmid histone shuffle assay (Figures S4C–S4E). Lastly, the histone clusters *HTA2B2* and *HHF1T1* were subcloned into superloser plasmid (pMAH316) to construct the *S. eubayanus* based histone shuffle strain.

SWR1 CRISPR/Cas9 deletions

We deleted the coding sequence of *SWR1* from the histone shuffle strain using CRISPR/Cas9 genome editing as previously described.[31] A targeting guide RNA plasmid was co-transformed with a donor template into a strain expressing Cas9 (Cas9 plasmid, pNA0519; and sgRNA expressing plasmid, pMAH269). Successful editing is indicated by the reduced killing phenotype of the guide RNA plasmid upon the addition of a donor template. We observed successful editing in 100% of the clones examined by PCR genotyping (Figure S3A). *swr1Δ* histone Humanized strains were generated as described above.

Mapping the inviability of macroH2A1 histone fold

To map the residues of macroH2A1-HF inviable in yeast, we first split the region corresponding to the core histone fold domain and C-terminal tail of macroH2A1 into seven arbitrary sub-regions (Figure S5B). We then swapped in these sub-regions of macroH2A1-HF into the chimeric fusion construct containing the *Hs*H2A and the N-terminal tail of macroH2A1-HF (pMAH338) and tested if each swapped-in region of macroH2A1-HF obstructed the function of the chimeric histone in *S. cerevisiae* (function as measure of the frequency of 5-FOA^R colonies following histone plasmid shuffle; sub-region 1, pMAH397; sub-region 2, pMAH399; sub-region 3, pMAH401; sub-region 4, pMAH403; sub-region 5, pMAH405; sub-region 6, pMAH407; sub-region 7, pMAH409). We first performed single sub-region swap experiments and found that sub-region 3 had the strongest negative effect on *Hs*H2A function (Figure S5D). Three additional sub-regions (two, four, and six) had less detrimental effects but were still significantly less fit than the base construct (Figure S5D). Combining these sub-regions in pairs (i.e., regions 2 + 3) resulted in total failure to complement (sub-regions 1 + 2, pMAH411; sub-regions 2 + 3, pMAH413; sub-regions 3 + 4, pMAH415; sub-regions 4 + 5, pMAH417; sub-regions 5 + 6, pMAH419; sub-regions 6 + 7, pMAH421), suggesting that multiple residues underly the inviability of macroH2A1-HF (Figure S5D).

We then performed single residue swap-backs within each inviable sub-region to identify the specific residues responsible for the inviability of macroH2A1-HF. These experiments were carried out as "swap to rescue" (See Table S1 for detailed plasmid list), where we swapped each residue within the inviable sub-regions of macroH2A1-HF back to the *Hs*H2A residue (Figures S5E–S5I).

For sub-region 3, we mapped the entirety of the inviability to residue Tyr38, which is part of the L1-loop interaction between H2A-H2B dimers (Figure S5E).[17,78] Furthermore, introducing the Tyr38Glu swapback into the various inviable sub-regions resulted in only a partial rescue to the viability of each (Figure S5F). For example, introducing Tyr38Glu significantly increased the average 5-FOA^R of Region 2 from 2.63e^{-6} to 3.52e^{-5} (Figure S5F). However, for sub-region four, introducing Try38Glu did not significantly improve the average 5-FOA^R (from 7.97e^{-6} to 4.05e^{-6}; Figure S5F). These data argue that Try38Glu swap-back alone is necessary but insufficient to rescue the inviability of macroH2A1-HF. By continuing to map the inviable residues for sub-regions two, four, and six, we identified a set of inviable residues from sub-regions two and four, but could not distinguish any one residue for region six (Figures S5G–S5I).

MNase digestions and sequencing

Yeast strains were grown overnight at 30°C in YPD to saturation. The following day, cultures were diluted to an A_{600} of 0.2 in 100 mL YPD media and grown to an A_{600} 0.8–1.0 at 30°C. Cells were then cross-linked by adding 2.7 mL of Formalin (final concentration of 1%) and incubated at 25°C with shaking for 15 min. To quench the formaldehyde, 5 mL of 2.5 M glycine was added and incubated for 5 min. Cells were then collected with centrifugation at 3000 x g for 5 min at 4°C and washed twice with ice-cold water. Pellets were immediately processed or snap-frozen with liquid nitrogen and stored at −80°C.

Cells were resuspended in 1 mL of spheroplasting buffer (1.2 M sorbitol, 100 mM potassium phosphate pH 7.5, 1 mM $CaCl_2$), with freshly added β-mercaptoethanol (0.5 mM) and 1 mg/mL Zymolyase 100T. Zymolyase digestions were monitored for production of spheroplasts. Spheroplast were collected by centrifugation at 3000 x g for 5 min, washed once in spheroplasting buffer and resuspended in 500 μL of MNase digestion buffer (1M sorbitol, 50 mM NaCL, 10 mM TRIS-HCL (pH 7.4), 5 mM MgCL2, 0.5 mM spermidine, 0.075% NP-40, with freshly added β-mercaptoethanol (1 mM) and either 2 units/mL or 0.2 units/mL MNase). Reactions were incubated for 45 min at 37°C and stopped by adding 16.6 μL of 0.5 M EDTA (30 mM final). Crosslinks were reversed by adding 12.5 μL 20% SDS (0.5% final), 12.5 μL proteinase K (20 mg/mL), and incubated for 1 h at 37°C and 2 h at 65°C. Digested DNA was extracted with two rounds of phenol-chloroform extraction, and DNA was precipitated with isopropanol. DNA was resuspended in TE buffer with 1 mg/mL RNAse A and incubated at 37°C for 30 min. Finally, DNA was purified with the Zymo DNA clean and concentrator kit according to the manufacturer's specifications.

Digested DNA was used as the input for Illumina library preps using the NEB Ultra II kit following the manufacturer's specification. Libraries were sequenced on an Illumina NextSeq 500 with paired-end 2 × 150 bp read chemistry. We generated approximately 21 million reads per sample.

Capillary electrophoresis and NRL estimate

Approximately 20 ng of MNase digested DNA was analyzed using the Agilent ZAG DNA analyzer system with the ZAG 135 dsDNA kit (1–1500 bp). The fragment length data was analyzed in MATLAB. Oligonucleosome sizes (up to penta-nucleosomes) were estimated using the 'findpeaks' function in the signal processing toolbox. Nucleosome repeat length was calculated as the slope of the line passing through the estimated oligonucleosome lengths.

MNase sequencing data analysis

Demultiplexed reads were first analyzed with Trimmomatic (v0.39)[61] to remove sequencing adaptors and then with FastQC (v0.11.4) to assess read quality. Processed reads were then aligned to the Scer3 genome (R64) using the Burrows Wheeler aligner (BWA) mem algorithm (v0.7.7).[62] For the mononucleosome analysis, we filtered reads with estimated insert sizes in the 120–180 bp range using SAMtools.[59] Filtered reads were then used as input for mononucleosome analysis using the DANPOS (v2) pipeline.[63] For the nucleosome occupancy analysis in Figure 4, we examined 70,592 nucleosomes for the *Hs*H2Amacro1.2 to *Sc* histones comparison; 71,177 nucleosomes for the macroH2A1-HF-sb to *Sc* histones comparison; and 70,679 nucleosomes for the *Hs*H2A to *Sc* histones comparison. Nucleosome peaks, binned at 10 bp, were called using the 'Dpos' algorithm to call positions relative to the WT samples. Next, mono-nucleosome occupancies were assessed using the 'Profile' algorithm relative to previously determined transcription start sites of 5206 genes.[45] We then clustered mono-nucleosome occupancies using k-means clustering (with k = 6), resulting in six classes of genes based on the relative positioning of nucleosomes from the TSS. The value of K was determined using the "elbow" method and using a previously defined number of clusters as a guide.[27] Next, we sorted the genes within each cluster by their *Z* score normalized RNAseq transcript abundance in WT yeast (Figure S7G). The nucleosome occupancies best clustered into six distinct groups, each exhibiting unique nucleosome phasing profiles (Figures S7G and S7H). Groups three and five showed poor phasing in WT and humanized yeast with *Hs*H2A, and were even less well phased in humanized yeast with either macroH2A1-HF-sb or H2Amacro1.2 (Figures S7G and S7H).

Nucleosome repeat length of each gene, relative to the +1 nucleosomes, was calculated by taking the slope of the line running from the mononucleosome fragment length to the pentanucleosome fragment length. We only consider those genes in groups 1, 2, 4, and 6, as those showed good phasing across all strains (Figures S7G and S7H). Density plots of these NRL values were generated in MATLAB using the 'ksdensity' function. To visualize the MNase-seq fragment lengths, we aligned processed reads to the Scer3 genome (R64) using Bowtie2 algorithm.[60] Alignments were down-sampled to ~2 million reads for each sample and then used to generate Vplots and profile plots using the R package VplotR.[64,79]

Lastly, we estimated locus-specific NRLs using the raw di-nucleosome fragment lengths from our MNase-seq data. First, reads were aligned using Minimap2 (options: -ax sr),[67] filtered based on the template length to analyze only di-nucleosome fragments (250 bp < template length <400 bp), and each alignment was split by genomic coordinates corresponding to protein-coding genes (n = 5801, excluding dubious ORFs and transposable elements). Next, the template lengths for each gene-specific alignment were extracted and fitted to a Gaussian distribution to estimate the gene-specific NRL. Lastly, for each gene, we then performed a pairwise comparison between the estimated average NRL ($n \geq 3$) using a two-tailed t test.

RNA extraction, sequencing, and nucleosome positioning analysis of differentially expressed genes

RNA was extracted and sequenced, and data was analyzed as previously described.[31] Libraries were sequenced on an Illumina NextSeq 500 with paired-end 2 × 150 bp read chemistry. We generated ~25 million reads per sample. Differentially expressed transcripts in either histone Humanized H2Amacro1.2 or macroH2A1-HF-sb were defined as log2 fold change >1 and <-1 with an adjusted p-value < 0.01 (a total of 572 genes). Gene enrichment analysis was done using the web tool ShinyGO (v 0.77).[80] Nucleosome occupancy of each gene (binned by 10 bp), relative to its transcription start site, was then sorted into clusters, as before, using k-means clustering. We excluded genes from clusters 3 and 5 as these genes did not exhibit well-phased nucleosomes, leaving us with 268 genes (114 up-regulated and 154 down-regulated). For each cluster, we determined the average relative nucleosome position for five nucleosomes downstream of the TSS in WT yeast (*Sc* histones). We then defined a window of 200 bp around each mean nucleosome position and then, using these coordinates, determined the position of the maximum peak for each nucleosome from every gene (totaling 684 nucleosomes for down-regulated genes and 924 nucleosomes for up-regulated genes). These positions were then plotted relative to the mean position for the wild-type nucleosome.

We then examined the percent change in nucleosome occupancy in the nucleosome-depleted region for all 5206 genes with annotated TSS. The NDR was defined as the region +50 bp from the −1 nucleosome to −50 bp from the +1 nucleosome (Figure S9B). We calculated the relative change in nucleosome occupancy to WT yeast (with *Sc* histones) as a percent change. We then examined NDR occupancy by sorting genes by their Z score normalized expression levels in WT yeast (Figures S9A and S9E). Lastly, we used the top and bottom 15% of most/least abundant genes to compare the relative log2FC expression changes in histone Humanized yeast relative to WT (Figures S9C and S9G). Protein-protein interactions (PPI) were determined by constructing a PPI network for the top 15% of genes using the String algorithm (Figures S9D and S9H).

HiC libraries and analysis

Cells were first grown to saturation in 10 mL YPD (overnight for *Sc* histone strain, ~3 days for *Hs* histone strain, and up to 7 days for the macroH2A's chimeric strains). Each was then subcultured into 150 mL of YPD at a starting A_{600} of 0.3 and grown until reaching A_{600} of ~0.8–1.0 (1.2×10^9 total cells). Cells were then crosslinked with formaldehyde (3% [v/v]) for 20 min at room temperature, and quenched with glycine (350 mM) for 15 min at 4°C. HiC experiments were then performed as previously described.[81,82] Complete details on HiC data generation and analysis can be found in Lazar-Stefanita et al..[44] The raw contact maps are available on our FigShare repository (See data and code availability statement).

Whole genome sequencing

Genomic DNA was extracted as previously described, and Illumina sequencing libraries were made using the NEB Ultra II FS kit.[31] Libraries were sequenced on an Illumina NextSeq 500 with paired-end 2 × 36 bp read chemistry, generating ~16 million reads per sample. Single nucleotide variant analysis (Table S3), ploidy levels, and chromosome coverage maps were generated as previously described.[31] In the H2Amacro1.2 histone Humanized yeast, we observed that all clones lost their mitochondrial genome (retaining a highly amplified mitochondrial origin of replication region), consistent with the overall worse growth of H2Amacro1.2 humanized yeast compared to macroH2A1-HF-sb strain (which didn't lose mitochondrial DNA). We filtered out genes with synonymous mutations to construct the String interaction network and used the remaining list of mutant genes as input queries. The interaction network was constructed using functional and physical protein associations, and the resulting network was clustered by MCL clustering with the inflation parameter set to 2. Breakpoint analysis of coverage data was done by thorough inspection in IGV genome browser.

Nanopore sequencing and analysis

Overnight yeast cultures of humanized macroH2A1-HF-sb clones 1 and 4 were pelleted (~5 mL), washed in 1 x PBS and resuspended in 5 mL of spheroplast buffer (1 M sorbitol, 50 mM potassium phosphate, 5 mM EDTA pH 7.5) supplemented with DTT (5mM) and zymolyase (50 mg/mL) and shaken at 210 rpm for 1 h at 30°C. Spheroplasts were centrifuged at 2,500 g at 4°C, gently washed with 1M sorbitol, and incubated in proteinase K solution (25 mM final EDTA, 0.5% SDS, Proteinase K 0.5 mg/mL) for 2 h at 65°C with gentle inversion every ~30 min. Lysates were extracted twice with a 1:1 ratio of Phenol:Chloroform:isoamyl alcohol and pooled aqueous layers were treated with ~10μg of RNase A for 30 min at 37°C before an additional 1:1 extraction with chloroform:isoamyl alcohol. DNA was precipitated with 1/10 volume 3M sodium acetate (pH 5.2) and 2.5X volume of ice-cold 100% ethanol and inverted until DNA strands visually appeared. High molecular weight DNA was spooled using a pipette tip, transferred to a new tube containing 70% ethanol wash, dried, and dissolved overnight in TE buffer (10 mM Tris-HCl pH 8.0, 1 mM EDTA).

High molecular weight gDNA was quantified using Qubit 1x dsDNA HS Assay reagent (Thermo, Q33231) on the Qubit flex Fluorometer. DNA samples were simultaneously tagmented and barcoded using Oxford Nanopore Rapid Barcoding kit (SQK-RBK004)

according to the manufacturer's protocol. Barcoded samples were pooled, cleaned, and concentrated with SERA-MAG beads (Cytiva, 29343052). The library was immediately loaded onto a Minion R9.4.1 flow cell (SKU: FLO-MIN106.001) and sequenced using the Gridion Mk1 device for 46 h.

Base calls were made with the Guppy high-accuracy model (v6.2.11). We sequenced to a depth of 21.5x for clone 1 and 42.6x for clone 4, with read N50's of 12,279 bp and 12,999 bp, respectively, allowing us to confidently infer the breakpoints across most repetitive Ty elements (typically ~6 kb). Reads were trimmed to remove barcode adaptors with Porechop and then aligned to the R64-2 Scer genome assembly using the Minimap2 aligner.[67] The quality of alignments was assessed with Alfred,[70] confirming a high proportion of reads with secondary alignments (15.2% and 23.5% of the total for clone 1 and clone 4, respectively). Structural variants were then called using the Sniffles[68] and CuteSV[80] programs, and the resulting vcf files were manually merged. Circos plots displaying chromosome coverage and translocations were made using the TBtools software package.[65] The rearrangement regions were analyzed using the Samplot program[66] to visualize non-contiguous mapping reads.